Large liquid detectors in Europe

A Scientific Case

J-E Campagne*, A. Bueno†, L. Oberauer‡
J. Bouchez*, J. Busto*, Ch. Cavata*, S. Davidson*, A. de Bellefon*, J. Dumarchez*,
S. Katsanevas*, M. Mezzetto*, L. Mosca*, T. Patzak*, A. Tonazzo*, C. Volpe*,
J. Äystö‡, L. Bezrukov‡, T. Enqvist‡, F. von Feilizsch‡, M. Göger-Neff‡, C. Hagner‡,
K. Hochmuth‡, T. Lachenmaier‡, M. Lindner‡, L. Oberauer‡, J. Peltuniemi‡, W. Potzel‡
G. Raffelt‡, T. Marrodán Undagoitia‡, M. Wurm‡, R. Zimmermann‡,
A. Badertscher†, A. Bueno†, A. Ereditato†, S. Gninenko†, W. Gruber†, L. Knecht†,
M. Laffranchi†, A. Meregaglia†, M. Messina†, A. Müller†, G. Natterer†, P. Otiougova†,
A. Rubbia†, N. Spooner†, J. Ulbricht†, A. Zalewska†
List of authors to be completed as well as the order policy

June 22, 2006

Abstract

A status report on the physics potential of the large scaled detectors as Water Čerenkov (MEMPHYS), Liquid Argon TPC (GLACIER) and Liquid Scintillator (LENA) is presented covering both the non-accelerator and accelerator topics.

*MEMPHYS
†GLACIER
‡LENA

Contribution to discussion for a European Funding request.

Contents

1 Introduction

The pioneer Water Čerenkov detectors (IMB, Kamiokande) were built to look for nucleon decay, a prediction of Grand Unified Theories. Unfortunately, no discovery was made in this field and the neutrino physics has been the bread and butter since the beginning of running time of these detectors. Just to remind the glorious past: first detection of a supernova neutrino explosion (SN1987A) [1, 2, 3, 4] acknowledged by the Nobel prize for Koshiba, Solar [5] and atmospheric anomalies discovery [6, 7] which have been explained as mass & mixing of the neutrinos, the latter being confirmed by the first long base line neutrino beam, i.e. the K2K experiment [8].

The proposed detectors GLACIER[1] [9], LENA[2] [10, 11] and MEMPHYS[3] [12], using different techniques will push the discovery frontiers on several domains: nucleon decay, supernova neutrinos (burst from sudden explosion or diffuse halo from past explosions), solar and atmospheric neutrinos, neutrinos from the Earth interior (geo-neutrinos), accelerator made neutrinos, indirect dark matter search... These items are reviewed in the following sections after a brief description of the key parameters of the detectors while the underground sites envisaged are described in section 4.

2 Brief detector description

The three detectors basic parameters are listed in Tab. 1. All these detectors are tens to hundreds of kilo tons mass all together of active target and situated in underground laboratories to be protected against background induced by cosmic rays. The large size of these detectors is motivated by the extremely low cross sections of neutrinos and/or the rareness of the interesting events. Some details of the detectors are discussed in the following sections while the Underground site related matter is discussed in section 4.

2.1 Liquid Argon TPC

GLACIER (Fig. 1) is the foreseen extrapolation up to 100 kT of a Liquid Argon Time Projection Chamber. A summary of parameters are listed in Tab. 1. The detector can be mechanically subdivided into two parts: (1) the liquid argon tanker and (2) the inner detector instrumentation. For simplicity, we assume at this stage that the two aspects can be decoupled.

The basic design parameters can be summarized as follows:

1. Single 100 kton "boiling" cryogenic tanker with Argon refrigeration (in particular, the cooling is done directly with Argon, e.g. without nitrogen)

[1] Giant Liquid Argon Charge Imaging ExpeRiment
[2] Low Energy Neutrino Astronomy
[3] MEgaton Mass PHYSics

	GLACIER	LENA	MEMPHYS
Detector dimensions			
type	vertical cylinder	horizontal cylinder	$3 \div 5$ shafts
diam. x length	$\phi = 70\text{m} \times L = 20\text{m}$	$\phi = 30\text{m} \times L = 100\text{m}$	$(3 \div 5) \times (\phi = 65\text{m} \times H = 65\text{m})$
typical mass (kt)	100	50	$440 \div 730$
Active target and readout†			
type of target	liquid argon (boiling)	phenyl-o-xylyethane	water (option: 0.2% $GdCl_3$)
readout type			
e^- drift	2 perp. views, 10^5 channels, ampli. in gas phase	12,000 20" PMTs $\gtrsim 20\%$ coverage	81,000 12" PMTs $\sim 30\%$ coverage
Č light	27,000 8" PMTs, $\sim 20\%$ coverage		
Scint. light	1,000 8" PMTs		

Table 1: Some basic parameters of the three detector baseline designs. The underground laboratory related matter are described in section 4 To be completed

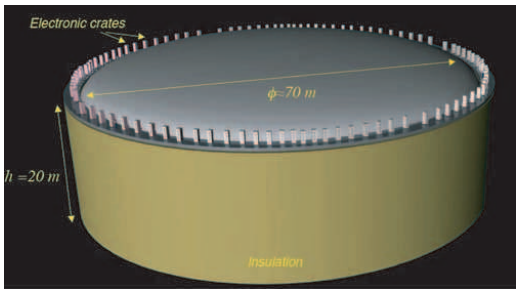

Figure 1: An artistic view of a 100 kton single tanker liquid argon detector. The electronic crates are located at the top of the dewar.

2. Charge imaging + scintillation + Čerenkov light readout for complete event information

3. Charge amplification to allow for extremely long drifts: the detector is running in bi-phase mode. In order to allow for long drift (≈ 20 m), we consider charge attenuation along drift and compensate this effect with charge amplification near the anodes located in gas phase.

4. Possibility of adding a magnetic field.

The inner detector instrumentation is made of: a cathode, located near the bottom of the tanker, set at -2 MV that creates a drift electric field of 1 kV/cm over the distance of 20 m. In this field configuration ionization electrons are moving upwards while ions are going downward. The electric field is delimited on the sides of the tanker by a series of ring electrodes (race-tracks) put at the appropriate voltages (voltage divider). The breakdown voltage of liquid argon is such that a distance of about 50 cm to the grounded tanker volume is electrically safe. For the high voltage we consider two solutions: (1) either the HV is brought inside the dewar through an appropriate custom-made HV feed-through or (2) a voltage multiplier could be installed inside the cold volume.

The tanker contains both liquid and gas argon phases at equilibrium. Since purity is a concern for very long drifts of the order of 20 meters, we think that the inner detector should be operated in bi-phase mode, namely drift electrons produced in the liquid phase are extracted from the liquid into the gas phase with the help of an appropriate electric field. Our measurements show that the threshold for 100% efficient extraction is about 3 kV/cm. Hence, just below and above the liquid two grids define the appropriate liquid extraction field. In addition to charge readout, we envision to locate PMTs around the tanker. Scintillation and Čerenkov light can be readout essentially independently. One can profit from the ICARUS R&D which has shown that PMTs immersed directly in the liquid Argon is possible[13]. One is using commercial Electron Tubes 8" PMTs with a photocathode for cold operation and a standard glass window. In order to be sensitive to DUV scintillation, the PMT are coated with a wavelength shifter (Tetraphenyl-Butadiene).

Summarizing about 1000 immersed phototubes with WLS would be used to identify the (isotropic and bright) scintillation light. While about 27000 immersed 8"-phototubes without WLS would provide a 20% coverage of the surface of the detector. As already mentioned, these latter should have single photon counting capabilities in order to count the number of Čerenkov photons.

2.2 Liquid Scintillator

The LENA detector is cylindrical in shape, with a length of about 100 m and 30 m diameter (Fig. 2 and Tab. 1). An inside part of 13 m radius contains approximately $5 \times 10^7\,\mathrm{m}^3$ of liquid scintillator while the outside part is filled with water to act as a muon veto. Both the outer and the inner volume are enclosed in steel tanks of 3 to 4 cm wall thickness. For most purposes, a fiducial volume at 1 m distance to the inner tank walls is defined, corresponding to 88 % of the inner detector volume.
The detectors axis is aligned horizontally. A tunnel-shaped cavern harbouring the detector is well feasible at most locations. In respect to accelerator physics, the axis should be oriented towards the neutrino source (e.g. CERN) in order to contain the full length of muon and electron tracks.
The default setting for light detection in the inner detector is the mounting of 12 000 photomultipliers (PMs) of 20" diameter each to the inner cylinder wall, which cover about 30 % of the surface. As an option, light concentrators can be installed in front of the PMs, increasing the surface coverage c to values of more than 50 %. Alternatively, $c = 30\,\%$ can be reached by the equipment of 8" PMs with light concentrators, thereby reducing costs compared to the default setting. Additional PMs are supplied in the outer muon veto to detect the Cherenkov light of incoming particles.
Possible candidates for the liquid scintillator are (1.) pure PXE (phenyl-xylyl-ethane), (2.) a mixture of 20 % PXE and 80 % Dodecane, or (3.) Linear Alkylbenzene (LAB). All three liquids are of minor toxicity to the environment and provide high flash and inflammation points.

1. PXE ($C_{16}H_{18}$, $\rho \simeq 0.985\,\mathrm{g/cm}^3$) has already been tested in the Counting Test Facility of the BOREXINO experiment. Combining the CTF data [14] with results of laboratory measurements done both in Heidelberg and in Munich [15], a light yield of about 10^4 photons/MeV can be reached by adding 6 g/l PPO 20 mg/l bisMSB as primary and secondary fluors that shift the scintillation light to 430 nm. At this wavelength, attenuation lengths of up to 12 m can be achieved after purification of PXE in an aluminum column [14]. For an event in the center of the LENA detector, a photoelectron (pe) yield of about $400c$ pe/MeV is therefore feasible.

2. The admixture of Dodecane ($C_{12}H_{26}$, $\rho \simeq 0.749\,\mathrm{g/cm}^3$) both lowers the light yield and increases the transparency of the scintillator. The effective photoelectron yield is comparable to the one of PXE up to about 80 mass percent of Dodecane. The

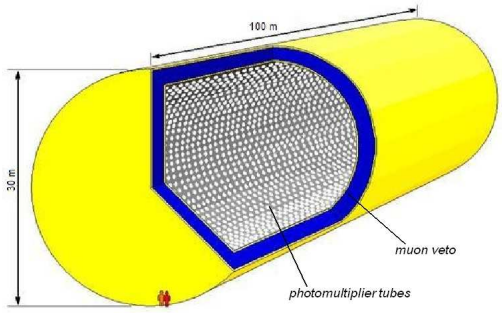

Figure 2: Sketch of the LENA detector.

resulting increase in the number of free protons and therefore in events due to the inverse beta decay of $\bar{\nu}_e$ is $\sim 26\,\%$.

3. LAB ($C_{17.6}H_{30}$, $\rho \simeq 0.862\,\mathrm{g/cm^3}$), a basic and therefore cheap ingredient of many detergents, has been tested as a liquid scintillator for the SNO+ experiment. Laboratory measurements done by the SNO collaboration show excellent light yield and transparency. Investigations in Munich are in preparation.

2.3 Water Čerenkov

The MEMPHYS detector (Fig. 3 and Tab. 1) is an extrapolation of Super-Kamiokande up to 730 kT. This Water Čerenkov detector is a collection of up to 5 shafts, and 3 are enough for 440 kt fiducial mass which is used hereafter. Each shaft is 65 m in diameter and 65 m height for the total water container dimensions, and this represent an extrapolation of a factor 4 with respect to the Super-Kamiokande running detector. The PMT surface defined as 2 m inside the water container is covered by about 81,000 12" PMTs to reach a 30% surface coverage equivalent to a 40% coverage with 20" PMTs. The fiducial volume is defined by an additional conservative guard of 2 m. The outer volume between the PMT surface and the water vessel is instrumented with 8" PMTs. If not contrary mentionned, the Super-Kamiokande analysis (efficiency, background reduction) [16] is used to compute the physcis potential of such a detector. In the US and in Japan, there are two competitors to MEMPHYS, namely UNO and Hyper-Kamiokande. These projects are similar in many respects and the hereafter presented physics potential may be transposed also for those detectors[4]. Currently, there is a very promising R&D activity concerning the possibility to introduce Gadolinium salt ($GdCl_3$) in side the 1 kT Water Čerenkov prototype of the K2K experiment. The physics goal is to decrease the background in many physics channels by tagging the neutron produced in the inverse beta decay interaction of $\bar{\nu}_e$ on free protons.

[4]Specific characteristics that are not identical to the projects concern the distance to accelerators or reactors

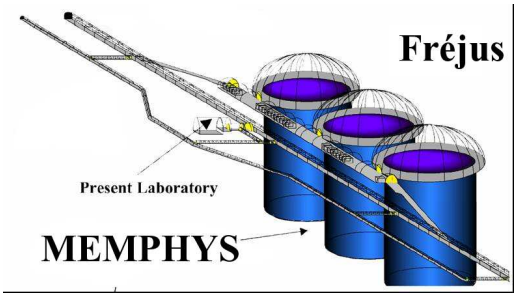

Figure 3: Sketch of the MEMPHYS detector under the Fréjus mountain (Europe).

For instance, 100 tons of $GdCl_3$ in Super-Kamiokande would yield more then 90% neutron captures on Gd [17].

3 Detector Perfomances

3.1 Proton decay sensitivity

For all relevant aspects of the proton stability in grand unified theories, in strings and in branes see reference [18].

Since proton decay is the most dramatic prediction coming from theories where the matter is unified, we hope to test those scenarios at future experiments. For this reason, a theoretical upper bound on the lifetime of the proton is very important to know about the possibilities of future experiments.

Recently a model-independent upper bound on the total proton decay lifetime has been pointed out [19]:

$$\tau_p^{upper} = \left\{ \begin{array}{ll} 6.0 \times 10^{39} & \text{(Majorana case)} \\ 2.8 \times 10^{37} & \text{(Dirac case)} \end{array} \right\} \times \frac{\left(M_X/10^{16} GeV\right)^4}{\alpha_{GUT}^2} \times \left(\frac{0.003 GeV^3}{\alpha}\right)^2 \text{ yrs} \quad (1)$$

where M_X is the mass of the superheavy gauge bosons. The parameter $\alpha_{GUT} = g_{GUT}^2/4\pi$, where g_{GUT} is the gauge coupling at the grand unified scale. α is the matrix element. See Fig. 4 and Fig. 5 for the present parameter space allowed by the experiments.

Most of the models (Supersymmetric or non-Supersymmetric) predict a lifetime τ_p below those upper bounds 10^{33-37} years, which are very interesting since it is the possible range of the proposed detectors.

In order to have an idea of the proton decay predictions, let us list in Tab. 2 the results in different models.

No specific simulation for MEMPHYS has been carried out yet. We therefore rely on the study done by UNO, adapting the results to MEMPHYS (which has an overall better coverage) when possible.

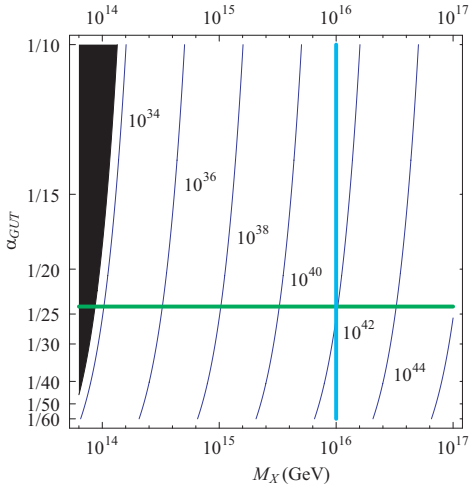

Figure 4: Isoplot for the upper bounds on the total proton lifetime in years in the Majorana neutrino case in the M_X–α_{GUT} plane. The value of the unifying coupling constant is varied from 1/60 to 1/10. The conventional values for M_X and α_{GUT} in SUSY GUTs are marked in thick lines. Experimentally excluded region is given in black [19].

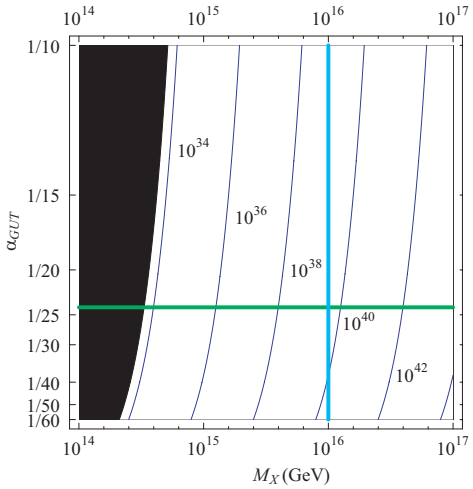

Figure 5: Isoplot for the upper bounds on the total proton lifetime in years in the Dirac neutrino case in the M_X–α_{GUT} plane. The value of the unifying coupling constant is varied from 1/60 to 1/10. The conventional values for M_X and α_{GUT} in SUSY GUTs are marked in thick lines. Experimentally excluded region is given in black [19].

Model	Decay modes	Prediction	References
Georgi-Glashow model	-	ruled out	[20]
Minimal realistic non-SUSY $SU(5)$	all channels	$\tau_p^{upper} = 1.4 \times 10^{36}$	[21]
Two Step Non-SUSY SO(10)	$p \to e^+\pi^0$	$\approx 10^{33-38}$	[22]
Minimal SUSY $SU(5)$	$p \to \bar{\nu}K^+$	$\approx 10^{32-34}$	[23]
SUSY $SO(10)$ with 10_H, and 126_H	$p \to \bar{\nu}K^+$	$\approx 10^{33-36}$	[24]
M-Theory(G_2)	$p \to e^+\pi^0$	$\approx 10^{33-37}$	[25]

Table 2: Summary of some recent predictions on proton partial lifetimes.

Due to its excellent imaging and energy resolution, GLACIER has the potentiality to discover nucleon decay in an essentially background-free environment. To understand the potential background contamination for this kind of search, we have carried out a detailed simulation of nucleon decays in Argon, i.e. including final state nuclear effects. This is vital since (1) they change the exclusive final state configuration and (2) they introduce a distortion of the event kinematics. Atmospheric neutrino and cosmic muon induced backgrounds have been fully simulated as well.

In order to quantitatively estimate the potential of the LENA detector for measuring the proton lifetime, a Monte Carlo simulation for the decay channel $p \to K^+\overline{\nu}$ has been performed. For this purpose, the Geant4 simulation toolkit has been used [26]. Not only all default Geant4 physics lists were included but also optical processes as scintillation, Cherenkov light production, Rayleigh scattering and light absorption. From these simulations a light yield of ~ 110 pe/MeV for an event in the center of the detector results. In addition, to take into account the so called quenching effects, the semi-empirical Birk's formula [27] has been introduced into the code.

3.1.1 $p \to e^+\pi^0$

Following UNO study, the detection efficiency of $p \to e^+\pi^0$ (3 showering rings event) is $\epsilon = 43\%$ for a 20 inch-PMT coverage of 40% or its equivalent, as envisioned for MEMPHYS. The corresponding estimated atmospheric neutrino induced background is at the level of 2.25 events/Mt.yr. From these efficiencies and background levels, proton decay sensitivity as a function of detector exposure can be estimated. A 10^{35} years partial lifetime (τ_p/B) could be reached at the 90% C.L. for a 5 Mt.yr exposure (10 yrs) with MEMPHYS (similar to case A in Fig. 6). Beyond that exposure, tighter cuts may be envisaged to further reduce the atmospheric neutrino background to 0.15 events/Mt.yr, by selecting quasi exclusively

the free proton decays.

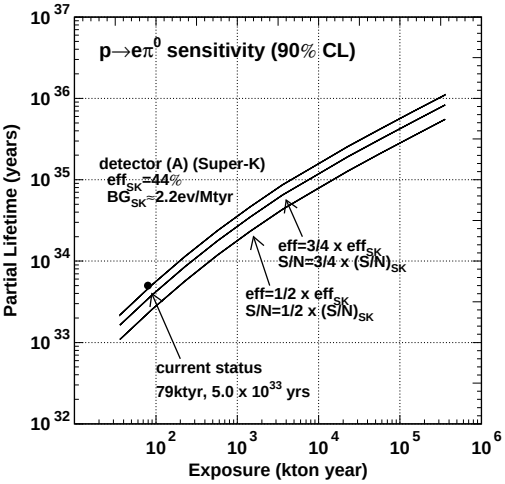

Figure 6: Sensitivity for $e^+\pi^0$ proton decay lifetime, as determined by UNO [28]. MEMPHYS corresponds to case (A).

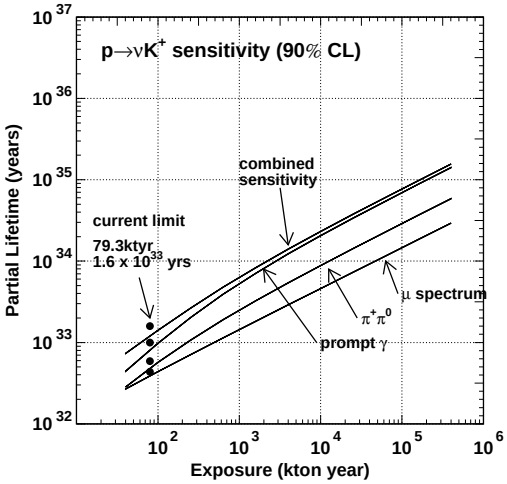

Figure 7: Expected sensitivity on νK^+ proton decay as a function of MEMPHYS exposure [28] (see text for details).

The positron and the two photons issued from the π^0 gives clear events in the GLACIER detector. We find that the π^0 is absorbed by the nucleus ∼45% of the times. Assuming a perfect particle and track identification, one may expect a 45% efficiency and a background level of 1 event/Mt.y. So, for a 1 Mt.yr (10 yrs) exposure with GLACIER one reaches $\tau_p/B > 0.5\ 10^{35}$ yrs at 90% C.L. (see Fig. 8).

In a liquid scintillator detector the decay $p \to e^+\pi^0$ will produce a $\sim$ 938 MeV signal coming from e^+ and π^0 showers. Only atmospheric neutrinos are expected to cause background events in this energy range. Using the fact that showers from both e^+ and π^0 propagate ∼4 m in opposite directions before being stopped, atmospheric neutrino background can be reduced. Applying this method, the current limit for this channel ($\tau_p/B = 5.4\ 10^{33}$ y [29]) could be improved.

3.1.2 $p \to \overline{\nu}K^+$

In LENA, proton decay events via the mode $p \to K^+\overline{\nu}$ have a very clear signature. The kaon causes a prompt monoenergetic signal (T=105 MeV) and from the kaon decay there is a short-delayed second monoenergetic signal, bigger than the first one. The kaon has a lifetime of $\tau(K^+) = 12.8$ ns and two main decay channels: with a probability of 63.43 % it decays via $K^+ \to \mu^+\nu_\mu$ and with 21.13%, via $K^+ \to \pi^+\pi^0$.

Simulations of proton decay events and atmospheric neutrino background has been performed and a pulse shape analysis has been applied. From the analysis an efficiency of

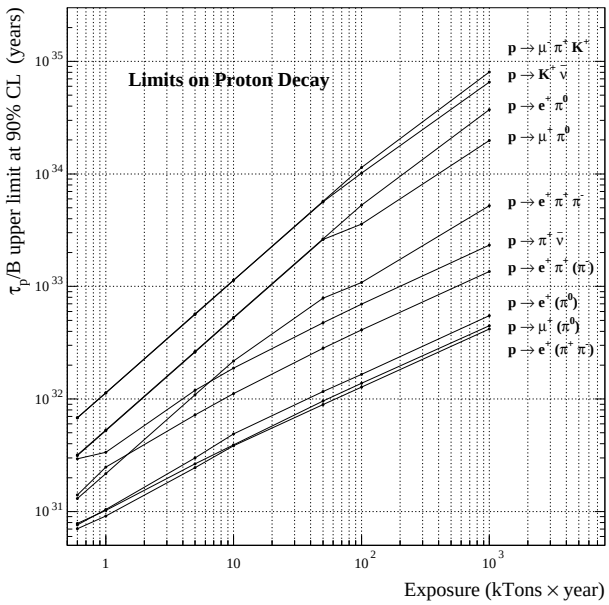

Figure 8: Expected proton decay lifetime limits (τ/B at 90% C.L.) as a function of exposure for GLACIER.

65% for the detection of a possible proton decay has been determined and a background suppression of $\sim 2\ 10^4$ has been achieved [11]. A detail study of background implying pion and kaon production in atmospheric neutrino reactions has been performed leading to a background rate of 0.064 y^{-1} due to the reaction $\nu_\mu + p \to \mu^- + K^+ + p$.

For the current proton lifetime limit for the channel considered ($\tau_p/B = 2.3\ 10^{33}$ y) [30], about 40.7 proton decay events would be observed in LENA after a measuring time of ten years with less than 1 background event. If no signal is seen in the detector within this ten years, the lower limit for the lifetime of the proton will be placed at $\tau_p/B > 4\ 10^{34}$ y at 90% C.L.

GLACIER uses dE/dx versus range as discriminating variable in a Neural Net to obtain the particle identity. We expect less than 1% of kaons mis-identified as protons. In this channel, the selection efficiency is high (97%) for a low background < 1 event/Mt.y. In case of absence of signal, we expect to reach $\tau_p/B > 1.1\ 10^{35}$ yrs at 90% C.L. for 1 Mt.y (10 years) exposure (see Fig. 8).

For the MEMPHYS detector, one should rely on the detection of the decay products of the K^+ since its momentum (360 MeV) is below the water Čerenkov threshold (ie. 570 MeV): a 256 MeV/c muon and its decay electron (type I) or a 205 MeV/c π^+ and π^0 (type II), with the possibility of a delayed (12 ns) coincidence with the 6 MeV ^{15}N

	GLACIER	LENA	MEMPHYS
$e^+\pi^0$			
ϵ(%)/Bkgd(Mt.y)	45/1	-	43/2.25
τ_p/B (90% C.L., 10 yrs)	0.5×10^{35}	-	1.0×10^{35}
$\bar{\nu}K^+$			
ϵ(%)/Bkgd(Mt.y)	97/1	65/1	8.8/3
τ_p/B (90% C.L., 10 yrs)	1.1×10^{35}	0.4×10^{35}	0.2×10^{35}

Table 3: Summary of the $e^+\pi^0$ and $\bar{\nu}K^+$ discovery potential by the three detectors. The $e^+\pi^0$ channel is not yet simulated in LENA.

de-excitation prompt γ (Type III). Using the imaging and timing capability of Super-Kamiokande, the efficiency for the reconstruction of $p \to \overline{\nu}K^+$ is $\epsilon = 33\%$ (I), 6.8% (II) and 8.8% (III), and the background is at 2100, 22 and 6 events/Mt.yr level. For the prompt γ method, the background is dominated by mis-reconstruction. As stated by UNO, there are good reasons to believe that this background can be lowered by at least a factor 2 corresponding to the atmospheric neutrino interaction $\nu p \to \nu \Lambda K^+$. In these conditions, and using Super-Kamiokande performances, a 5 Mt.yr MEMPHYS exposure would allow to reach $\tau_p/B > 2\ 10^{34}$ yrs (see Fig. 7).

3.1.3 Comparison between the detectors

Preliminary comparisons have been done between the detectors (Tab. 3). For the $e^+\pi^0$ channel, the Čerenkov detector gets a better limit due to their higher mass. However it should be noted that GLACIER, although five times smaller in mass than MEMPHYS, gets an expected limit that is only a factor two smaller. Liquid argon TPCs and liquid scintillator detectors get better results for the $\bar{\nu}K^+$ channel, due to their higher detection efficiency. The two techniques look therefore quite complementary and it would be worth to investigate deeper the pro and cons of each techniques with other channels not yet addressed by the present study as $e^+(\mu^+) + \gamma$ and neutron decays.

3.2 Supernova neutrinos

A supernova (SN) neutrino detection represents one of the next frontiers of neutrino astrophysics. It will provide invaluable information on the astrophysics of the core-collapse explosion phenomenon and on the neutrino mixing parameters. In particular, neutrino flavor transitions in the SN envelope are sensitive to the value of θ_{13} and on the type of mass hierarchy, and the detection of SN neutrino spectra at Earth can significantly contribute to sharpen our understanding of these unknown neutrino parameters. On the other hand, a detailed measurement of the neutrino signal from a galactic SN could yield important clues on the SN explosion mechanism.

3.2.1 SN neutrino emission and oscillations

A core-collapse supernova marks the evolutionary end of a massive star ($M \gtrsim 8\,M_\odot$) which becomes inevitably instable at the end of its life: it collapses and ejects its outer mantle in a shock-wave driven explosion. The collapse to a neutron star ($M \simeq M_\odot$, $R \simeq 10$ km) liberates a gravitational binding energy, $E_B \approx 3 \times 10^{53}$ erg, released at $\sim 99\%$ into (anti)neutrinos of all the flavors, and only at $\sim$1% into the kinetic energy of the explosion. Therefore, a core-collapse SN represents one of the most powerful sources of (anti)neutrinos in the Universe.

In general, numerical simulations of supernova explosions provide the original neutrino spectra in energy and time F^0_ν. Such initial distributions are in general modified by flavor transitions in SN envelope, in vacuum (and eventually in Earth matter)

$$F^0_\nu \longrightarrow F_\nu \tag{2}$$

and must be convolved with the differential interaction cross section σ_e for electron or positron production, as well as with the detector resolution function R_e, and the efficiency ε, in order to finally get observable event rates:

$$N_e = F_\nu \otimes \sigma_e \otimes R_e \otimes \varepsilon \tag{3}$$

Regarding the initial neutrino distributions F^0_ν, a SN collapsing core is roughly a black-body source of thermal neutrinos, emitted on a timescale of $\sim$ 10 s. Energy spectra parametrization are typically cast in the form of quasi-thermal distributions, with typical average energies: $\langle E_{\nu_e} \rangle = 9 - 12$ MeV, $\langle E_{\bar{\nu}_e} \rangle = 14 - 17$ MeV, $\langle E_{\nu_x} \rangle = 18 - 22$ MeV, where ν_x indicates any non-electron flavor.

The oscillated neutrino fluxes arriving at Earth may be written in terms of the energy-dependent "survival probability" p ($\bar{p}$) for neutrinos (antineutrinos) as [31]

$$\begin{aligned} F_{\nu_e} &= p F^0_{\nu_e} + (1-p) F^0_{\nu_x} \\ F_{\bar{\nu}_e} &= \bar{p} F^0_{\bar{\nu}_e} + (1-\bar{p}) F^0_{\nu_x} \\ 4F_{\nu_x} &= (1-p) F^0_{\nu_e} + (1-\bar{p}) F^0_{\bar{\nu}_e} + (2+p+\bar{p}) F^0_{\nu_x} \end{aligned} \tag{4}$$

where ν_x stands for either ν_μ or ν_τ. The probabilities p and $\bar{p}$ crucially depend on the neutrino mass hierarchy and on the unknown value of the mixing angle θ_{13} as shown in Tab. 4.

3.2.2 SN neutrino detection

Galactic core-collapse supernovae are rare, perhaps a few per century. Up to now, supernova neutrinos have been measured only once during SN 1987A explosion in the Large Magellanic Cloud ($d = 50$ kpc). Due to the relatively small masses of the detectors operative at that time, only few events were detected (11 in Kamiokande [1, 2] and 8 in IMB [3, 4]). The three proposed large-volume neutrino detectors with a broad range of science

Mass Hierarchy	$\sin^2\theta_{13}$	p	$\bar{p}$
Normal	$\gtrsim 10^{-3}$	0	$\cos^2\theta_{12}$
Inverted	$\gtrsim 10^{-3}$	$\sin^2\theta_{12}$	0
Any	$\lesssim 10^{-5}$	$\sin^2\theta_{12}$	$\cos^2\theta_{12}$

Table 4: Values of the p and $\bar{p}$ parameters used in Eq. 4 in different scenario of mass hierarchy and $\sin^2\theta_{13}$.

goals might guarantee continuous exposure for several decades, so that a high-statistics supernova neutrino signal may eventually be observed.

Expected number of events for GLACIER, MEMPHYS and LENA are reported in Tab. 5, for a typical galactic SN distance of 10 kpc. In the upper panel it is reported the total number of events, while the lower part refers to the ν_e signal detected during the prompt neutronization burst, with a duration of ~ 25 ms, just after the core bounce.

MEMPHYS		LENA		GLACIER	
Interaction	Rates	Interaction	Rates	Interaction	Rates
$\bar{\nu}_e$ IβD	2×10^5	$\bar{\nu}_e$ IβD	9×10^3	$\nu_e^{CC}(^{40}Ar, ^{40}K^*)$	2.5×10^4
$\overset{(-)}{\nu}_e{}^{CC}(^{16}O, X)$	10^4	ν_x pES	7×10^3	$\nu_x^{NC}(^{40}Ar^*)$	3.0×10^4
ν_x eES	10^3	$\nu_x^{NC}(^{12}C^*)$	3×10^3	ν_x eES	10^3
		ν_x eES	600	$\bar{\nu}_e^{CC}(^{40}Ar, ^{40}Cl^*)$	540
		$\bar{\nu}_e^{CC}(^{12}C, ^{12}B^{\beta^+})$	500		
		$\nu_e^{CC}(^{12}C, ^{12}N^{\beta^-})$	85		
Neutronization Burst rates					
MEMPHYS	60	ν_e eES			
LENA	~ 10	$\nu_e^{CC}(^{12}C, ^{12}N^{\beta^-})$			
GLACIER	380	$\nu_x^{NC}(^{40}Ar^*)$			

Table 5: Summary of the expected neutrino interaction rates in the different detectors for a $8M_\odot$ SN located at 10 kpc (Galactic center). The following notations have been used: IβD, eES and pES stands for Inverse β Decay, electron and proton Elastic Scattering, respectively. The final state nuclei are generally unstable and decay either radiatively (notation *), or by β^-/β^+ weak interaction (notation $^{\beta^{-,+}}$). The rates of the different reaction channels are listed, and for LENA they have been obtained by scaling the predicted rates from [32, 33].

One can realize that $\bar{\nu}_e$ detection by Inverse β Decay is the golden channel for MEMPHYS and LENA. In addition, the electron neutrino signal can be detected in LENA thanks to the interaction on ^{12}C. The three charged current reactions will deliver information on ν_e and $\bar{\nu}_e$ fluxes and spectra while the three neutral current reactions, sensitive to all neutrino flavours will provide information on the total flux. GLACIER has also the op-

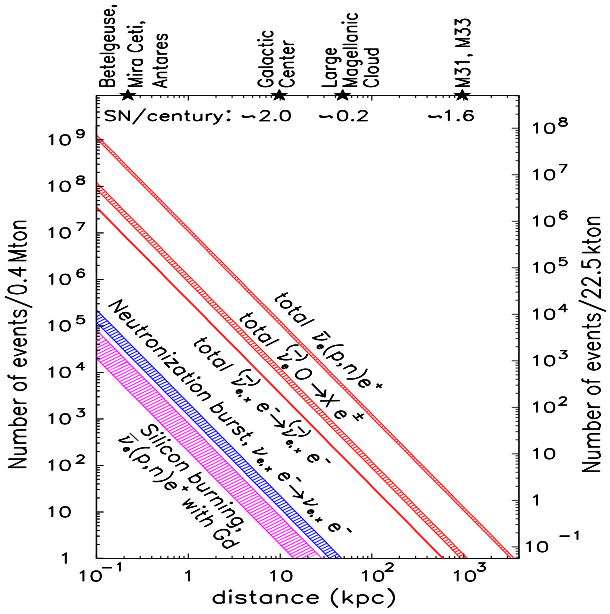

Figure 9: The number of events in a 400 kt water Čerenkov detector (left scale) and in SK (right scale) in all channels and in the individual detection channels as a function of distance for a supernova explosion [34].

portunity to see the ν_e by charged current interactions on ^{40}Ar with a very low threshold. The detection complementarity between ν_e and $\bar{\nu}_e$ is of great interest and would assure a unique way to probe SN explosion mechanism as well as neutrino intrinsic properties. Moreover, the huge statistics would allow spectral studies in time and in energy domain.

We stress that it will be difficult to establish SN neutrino oscillation effects solely on the basis of a $\bar{\nu}_e$ or ν_e "spectral hardening" relative to theoretical expectations. Therefore, in the recent literature the importance of model-independent signatures has been emphasized. Here we focus mainly on the signatures associated to: the prompt ν_e neutronization burst, the shock-wave propagation, the Earth matter crossing.

The analysis of the time structure of the SN signal during the first few tens of milliseconds after the core bounce can provide a clean indication if the full ν_e burst is present or absent and therefore allows one to distinguish between different mixing scenarios as indicated by the third column of Tab. 6. For example, if the mass ordering is normal and the θ_{13} is large, the ν_e burst will fully oscillate into ν_x. If θ_{13} is measured in the laboratory to be large, for example by one of the forthcoming reactor experiments, then one may distinguish between the normal and inverted mass ordering.

As discussed, MEMPHYS is mostly sensitive to the IβD, although the ν_e channel can be measured by the elastic scattering reaction $\nu_x + e^- \to e^- + \nu_x$ [35]. Of course, the identification of the neutronization burst is cleanest with a detector using the charged-current absorption of ν_e neutrinos, like GLACIER. Using its unique features to look at ν_e CC it is possible to probe oscillation physics during the early stage of the SN explosion, and using the NC it is possible to decouple the SN mechanism from the oscillation physics [36, 37].

A few seconds after core bounce, the SN shock wave will pass the density region in the stellar envelope relevant for oscillation matter effects, causing a transient modification of the survival probability and thus a time-dependent signature in the neutrino signal [38, 39]. It would show a characteristic dip when the shock wave passes [34], or a double-dip feature if a reverse shock occurs [40]. The detectability of such a signature has been studied in a Megaton Water Čerenkov detector like MEMPHYS by the IβD [34], and in a Large liquid Argon detector like GLACIER by Ar CC interactions [41]. The shock wave effects would be certainly visible also in a large volume scintillator like LENA. Of course, apart from identifying the neutrino mixing scenario, such observations would test our theoretical understanding of the core-collapse SN phenomenon.

One unequivocal indication of oscillation effects would be the energy-dependent modulation of the survival probability $p(E)$ caused by Earth matter effects [42]. The Earth matter effects can be revealed by wiggles in energy spectra and LENA benefit from a better energy resolution than MEMPHYS in this respect which may be partially compensated by 10 times more statistics [43]. The Earth effect would show up in the $\bar{\nu}_e$ channel for the normal mass hierarchy, assuming that θ_{13} is large (Tab. 6). Another possibility to establish the presence of Earth effects is to use the signal from two detectors if one of them sees the SN shadowed by the Earth and the other not. A comparison between the signal normalization in the two detectors might reveal Earth effects [44]. The shock wave

Mass Hierarchy	$\sin^2\theta_{13}$	ν_e neutronization peak	Shock wave	Earth effect
Normal	$\gtrsim 10^{-3}$	Absent	ν_e	$\bar{\nu}_e$ ν_e (delayed)
Inverted	$\gtrsim 10^{-3}$	Present	$\bar{\nu}_e$	ν_e $\bar{\nu}_e$ (delayed)
Any	$\lesssim 10^{-5}$	Present	-	both $\bar{\nu}_e$ ν_e

Table 6: Summary of the neutrino properties effect on ν_e and $\bar{\nu}_e$ signals.

propagation can influence the Earth matter effect, producing a delayed effect $5-7$ s after the core-bounce, in some particular situations [45] (Tab. 6).

Exploiting these three experimental signatures, by the joint efforts of the complementarity SN neutrino detection in MEMPHYS, LENA, and GLACIER it would be possible to extract valuable information on the neutrino mass hierarchy and to put a bound on θ_{13}, as shown in Tab. 6.

Other interesting ideas has been also studied in literature, ranging from the pointing of a SN by neutrinos [46], an early alert for SN observatory exploiting the neutrino signal [47], and the detection of neutrinos from the last phases of a burning star [48].

Up to now, we have investigated SN in our Galaxy, but the calculated rate of supernova explosions within a distance of 10 Mpc is about 1 per year. Although the number of events from a single explosion at such large distances would be small, the signal could be separated from the background with the request to observe at least two events within a time window comparable to the neutrino emission time-scale ($\sim$ 10 sec), together with the full energy and time distribution of the events [49]. In a MEMPHYS detector, with at least two neutrinos observed, a supernova could be identified without optical confirmation, so that the start of the light curve could be forecasted by a few hours, along with a short list of probable host galaxies. This would also allow the detection of supernovae which are either heavily obscured by dust or are optically dark due to prompt black hole formation.

3.2.3 Diffuse Supernova Neutrino Background

A galactic Supernova explosion will be a spectacular source of neutrinos, so that a variety of neutrino and SN properties could be determined. However, only one such explosion is expected in 20 to 100 years. Alternatively, it has been suggested that we might detect the cumulative neutrino flux from all the past SN in the Universe, the so called Diffuse Su-

pernova Neutrino Background (DSNB) [5]. In particular, there is an energy window around $20 - 40$ MeV where the DSNB signal can emerge above other sources, so that proposed detectors may measure this flux after some years of exposure times.

The DSNB signal, although weak, is not only "guaranteed", but can also probe different physics from a galactic SN, including processes which occure on cosmological scales in time or space. This makes them complementary to electromagnetic radiation which is much easier to detect, but also much easier to be absorbed or scattered on its way.

For instance, the DSNB signal is sensitive to the evolution of the SN rate, which is closely related to the star formation rate [50, 54]. Additionally, neutrino decay scenarios with cosmological lifetimes could be analyzed and constrained [51], as proposed in [52].

An upper limit on the DSNB flux has been set by the Super-Kamiokande experiment [53]

$$\phi_{\bar{\nu}_e}^{\mathrm{DSNB}} < 1.2 \text{ cm}^{-2} \text{ s}^{-1} \qquad (E_\nu > 19.3 \text{ MeV}) \tag{5}$$

However most of the estimates are below this limit and therefore DSNB detection appears to be feasible only with the large detector foreseen, through $\bar{\nu}_e$ inverse beta decay in MEMPHYS and LENA detectors and through $\nu_e + {}^{40}Ar \rightarrow e^- + {}^{40}K^*$ (and the associated gamma cascade) in GLACIER [59].

Typical estimates for DSNB fluxes (see for example [54]) predict an event rate of the order of $(0.1 \div 0.5)$ cm^{-2} s^{-1} MeV^{-1} for energies above 20 MeV.

The DSNB signal energy window is constrained from above by the atmospheric neutrinos and from below by either the nuclear reactor $\bar{\nu}_e$ (I), the spallation production unstable radionuclei by cosmic ray muons (II), the decay of "invisible" muon into electron (III), and solar ν_e neutrinos (IV). The three detectors are affected differently these backgrounds.

GLACIER looking at ν_e is mainly affected by type IV. MEMPHYS filled with pure water is mainly affected by type III due to the fact that the muons may have not enough energy to produce Čerenkov light. As pointed out in [34], with addition of Gadolinium [17] the detection of the captured neutron releasing 8 MeV gamma after of the order of 20 μs (10 times faster than in pure water), would give the possibility to reject neutrinos other than $\bar{\nu}_e$ that is to say not only the "invisible" muon (type III) but also the spallation background (type II). LENA taking benefit from the delayed neutron capture in $\bar{\nu}_e + p \rightarrow n + e^+$, is mainly affected by reactor neutrinos (I) which impose to choose an underground site far from nuclear plants: if LENA is deployed at the Center for Underground Physics in Pyhäsalmi (CUPP, Finland), there will be an observational window from $\sim$ 9.5 to 30 MeV that is almost free of background. The expected rates of signal and background are presented in Tab. 7.

According to DSN models [54] that are using different SN simulations from the LL [55], TBP [56] and KRJ [57] groups for the prediction of the DSN energy spectrum and flux, a detection of the DSN in this energy regime with LENA seems all but certain. Within ten years, 20 to 230 events are expected, the exact number mainly depending on

[5] We prefer the "Diffuse" rather the "Relic" word to not confuse with the primordial neutrinos produced one second after the Big Bang.

Interaction	Exposure	Energy Window	Signal/Bkgd
1 shaft MEMPHYS + 0.2% Gd (with bkgd Kamioka)			
$\bar{\nu}_e + p \rightarrow n + e^+$ $n + Gd \rightarrow \gamma$ (8 MeV, 20 μs)	0.7 Mt.y 5 yrs	$[15 - 30]$ MeV	(43-109)/47
LENA at Pyhäsalmi			
$\bar{\nu}_e + p \rightarrow n + e^+$ $n + p \rightarrow d + \gamma$ (2 MeV, 200 μs)	0.4 Mt.y 10 yrs	$[9.5 - 30]$ MeV	(20-230)/8
GLACIER			
$\nu_e + {}^{40}Ar \rightarrow e^- + {}^{40}K^*$	0.5 Mt.y 5 yrs	$[16 - 40]$ MeV	(40-60)/30

Table 7: DSNB expected rates. The larger numbers are computed with the present limit on the flux by SuperKamiokande collaboration. The lower numbers are computed for typical models. The background coming from reator plants have been computed for specific locations for MEMPHYS and LENA. For MEMPHYS, the SuperKamiokande background has been scaled by the exposure. More studies are needed to estimate the background at the new Fréjus laboratory.

the uncertainties of the Star Formation Rate (SFR) in the near universe. Signal rates corresponding to three different DSN models and the background rates due to the reactor (I) and atmospheric neutrinos are shown in Fig. 10 for 10 years of measurement with LENA in CUPP.

Moreover, assuming the most likely rates of 2.8 to 5.5 DSN events per year, after a decade of measurement statistics in LENA might already be good enough to distinguish between the LL and the TBP model that give the most different predictions on the DSN's spectral slope and therefore event rates. This will give valuable constraints on the SN neutrino spectrum and explosion mechanism.

Finally, if one achieves a threshold below 10 MeV for the DSN detection it might be possible to get a glimpse at the low-energetic part of the spectrum that is dominated by neutrinos emitted by SNe at redshifts $z > 1$. About 25% of the DSN events in the observational window will be caused by these high-z neutrinos. This might provide a new way of measuring the SFR at high redshifts. At these distances, conventional astronomy looking for Star Formation Regions is strongly impeded by dust extinction of the UV light that is emitted by young stars. The z-sensitivity of the detector could be further improved by choosing a location far away from the nuclear power plants of the northern hemisphere. For instance, a near to optimum DSN detection threshold of 8.4 MeV could be realized by deploying LENA in New Zealand.

An analysis of the expected DSN spectrum that would be observed with a gadolinium-loaded Water Čerenkov detector has been carried out in [58]. The possible measurements of the parameters (integrated luminosity and average energy) of supernova $\bar{\nu}_e$ emission have

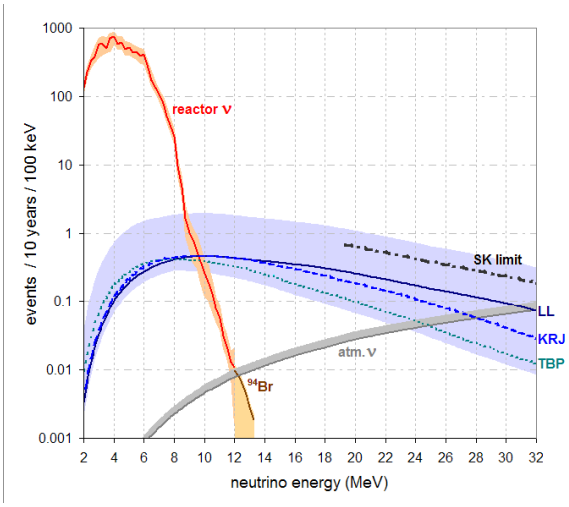

Figure 10: Diffuse supernova neutrino signal and background in LENA detector in 10 years of exposure. Shaded regions give the uncertainties of all curves. An observational window between ~ 9.5 to 30 MeV that is almost free of background can be identified.

been computed for 5 years running of a Gd-enhanced SuperKamiokande detector, which would correspond to 1 year of one Gd-enhanced MEMPHYS shaft. The results are shown in Fig. 11. Even if detailed studies on characterization of the background are needed, the DSN events may be as powerful as the measurement made by Kamioka and IMB with the SN1987A $\bar{\nu}_e$ events.

3.3 Solar neutrinos

In the past years Water Čherenkov detectors have measured the high energy tail ($E > 5$ MeV) of the solar ^{8}B neutrino flux using electron-neutrino elastic scattering [60]. Since such detectors could record the time of an interaction and reconstruct the energy and direction of the recoiling electron, unique information of the spectrum and time variation of the solar neutrino flux was extracted. This provided further insights into the "solar neutrino problem", the deficit of the neutrino flux (measured by several experiments) with respect to the flux expected by the standard solar models . It also constrained the neutrino flavor oscillation solutions in a fairly model-independent way.

With MEMPHYS, Super-Kamiokande's measurements obtained from 1258 days of data could be repeated in about half a year (the seasonal flux variation measurement requires of course a full year). In particular, a first measurement of the flux of the rare "hep" neutrinos may be possible. Elastic neutrino-electron scattering is strongly forward peaked. To separate the solar neutrino signal from the isotropic background events (mainly due to low radioactivity), this directional correlation is exploited. Angular resolution is limited

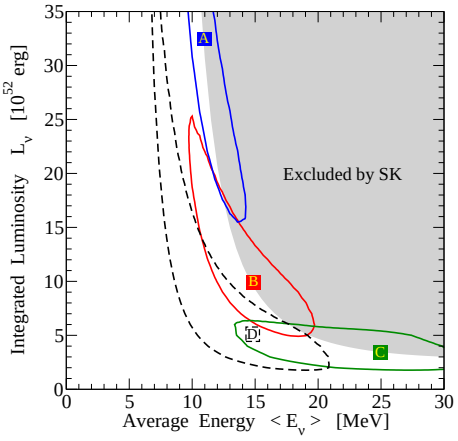

Figure 11: Possible 90% C.L. measurements of the emission parameters of supernova electron antineutrino emission after 5 years running of a gadolinium-enhanced SK detector or 1 year of one gadolinium-enhanced MEMPHYS shaft [58].

by multiple scattering. The reconstruction algorithm first reconstructs the vertex from the PMT times and then the direction assuming a single Cherenkov cone originating from the reconstructed vertex. Reconstructing 7 MeV events in MEMPHYS seems not to be a problem and decreasing the threshold would imply serious care of the detector radioactivity level as well as the laboratory environment as air free of radon (cf. SNO Laboratory). To be completed if needed by MEMPHYS...

With LENA, one would get a large amount of neutrinos from ^{7}Be, arround $\sim 5.4\,10^3$/day. Depending on the signal-to-background ratio, this would provide a sensitivity for time variations in the ^{7}Be neutrino flux of $\sim 0.5\%$ during one month of measuring time. Such a sensitivity may give information at a unique level on helioseismology (pressure or temperature fluctuations) and on a possible magnetic moment interaction with a timely varying solar magnetic field.

The *pep* neutrinos neutrinos are expected also to be recorded at a rate of 210/day, this would provide a better understanding the global solar neutrino luminosity. The neutrino flux from the CNO cycle is theoretically predicted only with the lowest accuracy (30%) of all solar neutrino fluxes. Therefore, LENA would provide a new opportunity for a detailed study of solar physics. However, the observation of such solar neutrinos in these detectors, through i.e. elastic scattering, is not a simple task, since neutrino events cannot be separated from the background, and it can be accomplished only if the detector contamination will be kept very low [61]. Moreover, only mono-energetic sources as such mentioned can be detected, taking advantage of the Compton-like shoulder edge produced in the event spectrum.

Recently, it has been investigated the possibility to register ^{8}B solar neutrinos by means

of the charged current interaction with the ^{13}C [62] nuclei naturally contained in organic scintillators. Even, if the event signal does not keep the directionality of the neutrino, it can be separated from the background by exploiting the time and space coincidence with the subsequent decay of the produced ^{13}N nuclei (remaining background of about 60/year corresponding to a redution factor of $\sim 3\ 10^{-4}$) [63]. Around 360 events of this type per year can be estimated for LENA. A deformation due to the MSW-effect should be observable in the low-energy regime after a couple of years of measurements.

For the proposed LENA location in Pyhäsalmi ($\sim$ 4000 m.w.e.), the cosmogenic background will be sufficiently low for the mentioned measurements. Notice that Fréjus location would be also good in this respect ($\sim$ 4800 m.w.e.). The radioactivity of the detector would have to be kept very low (10^{-17} g/g level U-Th) as in the KamLAND detector.

The solar neutrinos in GLACIER can be registered through the elastic scattering $\nu_x + e^- \rightarrow \nu_x + e^-$ (ES) and the absorption reaction $\nu_e + {}^{40}Ar \rightarrow e^- + {}^{40}K^*$ (ABS) followed by γs emission. Even if these reactions have low threshold (e.g 1.5 MeV for the second one), one expects to operate in practice with a threshold set at 5 MeV on the primary electron kinetic energy to reject background from neutron capture followed by gamma ray emission which constitute the main background in some underground laboratory [64] as for the LNGS (Italy). These neutrons are induced by the spontaneous fission of the cavern rock (note that in case of a salt mine this background may be significantly reduced).

The expected raw event rate is 330,000/year (66% from ABS, 25% from ES and 9% from neutron background induced events) assuming the above mentioned threshold on the final electron energy. Then, applying further offline cuts to purify separatly the ES sample and the ABS sample, one gets the rates shown on Tab. 8.

	Events/year
Elastic channel ($E \geq 5$ MeV)	45,300
Neutron bkgd	1,400
Absorption events contamination	1,100
Absorption channel (Gamow-Teller transition)	101,700
Absorption channel (Fermi transition)	59,900
Neutron bkgd	5,500
Elastic events contamination	1,700

Table 8: Number of events expected in GLACIER per year, compared with the computed background (no oscillation) in the Gran Sasso Laboratory (Italy) rock radioactivity condition (i.e. 0.32 10^{-6} n cm^{-2} s^{-1}($>$ 2.5 MeV). The Absorption channel have been split into the contributions of events from Fermi transition and from Gamow-Teller transition of the ^{40}Ar to the different ^{40}K excited levels and that can be separated using the emitted gamma energy and multiplicity

A possible way to combine the ES and the ABS channels similar to the NC/CC flux

ratio measured by SNO collaboration [65], is to compute the following ratio:

$$R = \frac{N^{ES}/N_0^{ES}}{\frac{1}{2}\left(N^{ABS-GT}/N_0^{ABS-GT} + N^{ABS-F}/N_0^{ABS-F}\right)} \tag{6}$$

where the numbers of expected events without neutrino oscillations are labeled with a 0). This double ratio has the following advantages: first it is independent of the ^{8}B total neutrino flux, predicted by different solar models, and second it is free of experimental threshold energy bias and of the adopted cross-sections for the different channels. With the present fit to solar and KamLAND data (see sec. 3.7), one expects a value of $R = 1.30 \pm 0.01$ after one year of data taking with GLACIER. The quoted error for R only takes into account statistics.

3.4 Atmospheric Neutrinos

Atmospheric neutrinos originates from the decay chain initiated by the collision of cosmic rays with the upper layers of the Earth's atmosphere. The hadronic interaction between primary cosmic rays (mainly protons and helium nuclei) and the light atmosphere nuclei produces secondary π and K mesons, which then decay giving electron and muon neutrinos and antineutrinos. At lower energies the main contribution comes from π mesons, and the decay chain $\pi \to \mu + \nu_\mu$ followed by $\mu \to e + \nu_e + \nu_\mu$ produces essentially two ν_μ for each ν_e. As the energy increases, more and more muons reach the ground before decays, and therefore the ν_μ/ν_e ratio increases. For $E_\nu \gtrsim 1$ GeV the dependence of the total neutrino flux on the neutrino energy is well described by a power law, $d\Phi/d_E \propto E^{-\gamma}$ with $\gamma = 3$ for ν_μ and $\gamma = 3.5$ for ν_e, whereas at sub-GeV energies the dependence becomes more complicated because of the effects of the solar wind and of the Earth's magnetic field [66]. As for the zenith dependence, for energies larger than a few GeV the neutrino flux is enhanced in the horizontal direction since pions and muons can travel a longer distance before reaching the ground, and therefore have more chances to decay producing neutrinos.

Historically, the atmospheric neutrino problem originated in the 1980's as a discrepancy between the atmospheric neutrino flux measured with different experimental techniques. In the previous years, a number of detectors had been built, which could detect neutrinos through the observation of the charged lepton produced in charged-current neutrino-nucleon interactions inside the detector itself. These detectors could be divided into two classes: *iron calorimeters*, which reconstructed the track or electromagnetic shower produced by the lepton, and *water Cerenkov*, which measured instead the Cerenkov light emitted by the lepton as it moved faster than light in water. The oldest iron calorimeters, Frejus [67] and NUSEX [68], found no discrepancy between the observed flux and the theoretical predictions, whereas the two water Cerenkov detectors, IMB [69] and Kamiokande [70], observed a clear deficit in the predicted ν_μ/ν_e ratio. The problem was finally solved in 1998, when the water Cerenkov detector Super-Kamiokande [71] established with high statistical accuracy that there was indeed a zenith- and energy-dependent deficit in the

muon neutrino flux with respect to the theoretical predictions, and that this deficit was compatible with the hypothesis of mass-induced $\nu_\mu \to \nu_\tau$ oscillations. Also, the independent confirmation of this effect from the iron calorimeter experiments Soudan-II [72] and MACRO [73] eliminated the discrepancy between the two experimental techniques.

Despite providing the first solid evidence for neutrino oscillations, atmospheric neutrino experiments have received only minor consideration during the last years. This is mainly due to two important limitations:

- the sensitivity of an atmospheric neutrino experiments is strongly limited by the large uncertainties in the knowledge of neutrino fluxes and neutrino-nucleon cross-section. Such uncertainties can be as large as 20%.

- in general, water Cerenkov detectors do not allow an accurate reconstruction of the neutrino energy and direction if none of the two is known "a priori". This strongly limits the sensitivity to Δm^2, which is very sensitive to the resolution on L/E.

During its phase-I, Super-Kamiokande has collected 4099 electron-like and 5436 muon-like contained neutrino events [74]. With only about a hundred events each, K2K [75] and Minos [76] already provide a stronger bound on the atmospheric mass-squared difference Δm^2_{31}. The present value of the mixing angle θ_{23} is still dominated by Super-Kamiokande data, being statistics the most important factor for such a measurement, but strong improvements are expected from the next generation of long-baseline experiments (T2K [77] and NOνA [78]).

Despite these drawbacks, atmospheric detectors can still play a leading role in the future of neutrino physics due to the huge range in energy (from 100 MeV to 10 TeV and above) and distance (from 20 km to more than 12000 Km) covered by the data. This unique feature, as well as the very large statistics expected for a detector such as MEMPHYS ($20 \div 30$ times the present SK event rate), will allow a very accurate study of *subdominant modifications* to the leading oscillation pattern, thus providing complementary information to accelerator-based experiments. More concretely, atmospheric neutrino data will be extremely valuable for:

- resolving the octant ambiguity: although future LBL experiments are expected to considerably improve the measurement of the absolute value of the small quantity $D_{23} \equiv \sin^2\theta_{23} - 1/2$, they will have practically no sensitivity on its sign. On the other hands, it has been pointed out [79] that the $\nu_\mu \to \nu_e$ conversion signal induced by the small but finite value of Δm^2_{21} can resolve this degeneracy. However, observing such a conversion requires a very long baseline and low energy neutrinos, and atmospheric sub-GeV electron-like events are particularly suitable for this purpose. In Fig. 12 we show the potential of different ATM+LBL experiments to exclude the octant degenerate solution.

- resolving the hierarchy degeneracy: if θ_{13} is not too small, matter effect will produce resonant conversion in the $\nu_\mu \leftrightarrow \nu_e$ channel for neutrinos (antineutrinos) if the mass

hierarchy is normal (inverted). The observation of this enhanced conversion would allow the determination of the mass hierarchy. Although a magnetized detector would be the best solution for this task, it is possible to extract useful information also with a conventional detector since the event rates expected for atmospheric neutrinos and antineutrinos are quite different. This is clearly visible from Fig. 13, where we show how the sensitivity to the mass hierarchy of different LBL experiments is drastically increased when the ATM data collected by the same detector are also included in the fit.

- measuring or improving the bound on θ_{13}: although atmospheric data alone are not expected to be competitive with the next generation of long-baseline experiments in the sensitivity to θ_{13}, they will contribute indirectly by eliminating the octant degeneracy, which is an important source of uncertainty for LBL. In particular, if $\theta_{23}^{\rm true}$ is larger than 45° then the inclusion of atmospheric data will considerably improve the LBL sensitivity to $\theta 13$, as can be seen from the right panel of Fig. 14.

- searching for physics beyond the Standard Model: the appearance of subleading features in the main oscillation pattern can also be a hint for New Physics. The huge range of energies probed by atmospheric data will allow to put very strong bounds on mechanisms which predict deviation from the $1/E$ behavior. For example, the bound on non-standard neutrino-matter interactions and on other types of New Physics (such as violation of the equivalence principle, or violation of the Lorentz invariance) which can be derived from *present* data is already the strongest which can be put on these mechanisms [80]. The increased statistics expected for MEMPHYS will further improve these constraints.

Finally, it is worth remembering that atmospheric neutrino fluxes are themselves an important subject of investigation, and at the light of the precise determination of the oscillation parameters provided by long-baseline experiments the atmospheric neutrino data accumulated by MEMPHYS can be used as a *direct measurement* of the incoming neutrino flux, and therefore as an indirect measurement of the primary cosmic rays flux.

3.5 Geo neutrinos

The total power dissipated from the Earth (heat flow) has been measured with thermal techniques to be 44.2 ± 1.0 TW. Despite this small quoted error, a more recent evaluation of the same data (assuming much lower hydrothermal heat flow near mid-ocean ridges) has led to a lower figure of 31 ± 1 TW. On the basis of studies of chondritic meteorites the calculated radiogenic power is thought to be 19 TW (about half of the total power), 84% of which is produced by ^{238}U and ^{232}Th decay which in turn produce $\bar{\nu}_e$ by β decays. It is then of prime importance to measure the $\bar{\nu}_e$ flux coming from the Earth to get geophysical information, with possible applications in the interpretation of the geomagnetism.

The KamLAND collaboration has recently reported the first observation of the geo-neutrinos [81]. The events are identified by the time and distance coincidence between

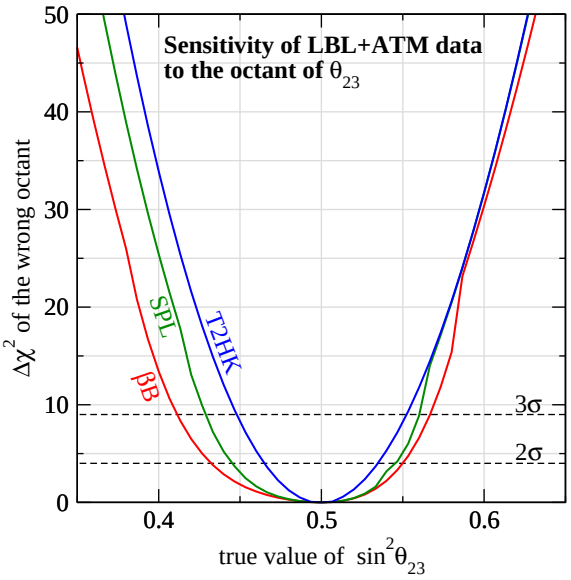

Figure 12: Discrimination of the wrong octant solution as a function of $\sin^2\theta_{23}^{\rm true}$, for $\theta_{13}^{\rm true}=0$. We have assumed 10 years of data taking with a 440-kton detector.

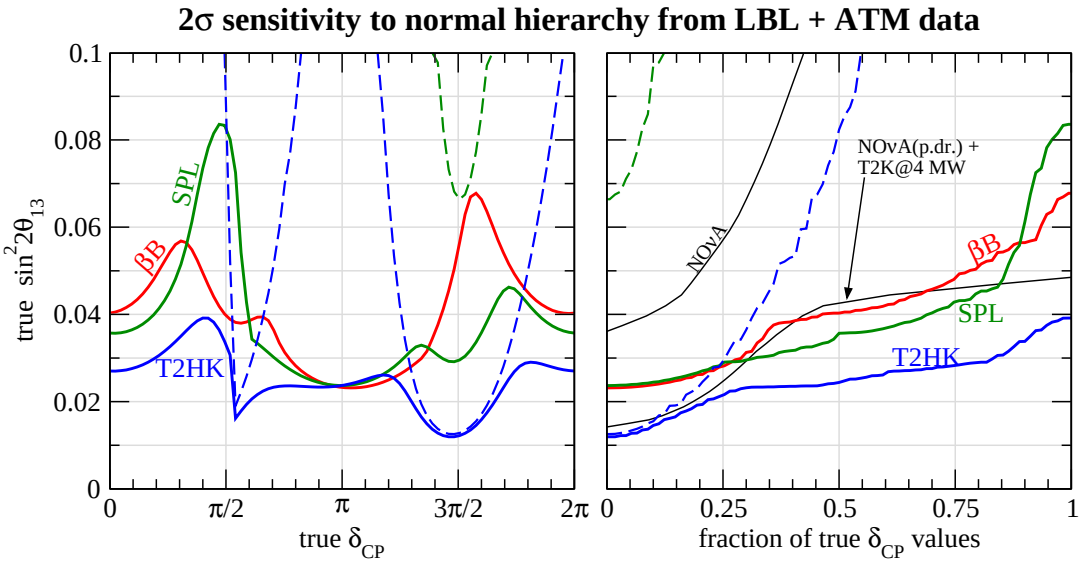

Figure 13: Sensitivity to the mass hierarchy at 2σ ($\Delta\chi^2=4$) as a function of $\sin^2 2\theta_{13}^{\rm true}$ and $\delta_{\rm CP}^{\rm true}$ (left), and the fraction of true values of $\delta_{\rm CP}^{\rm true}$ (right). The solid curves are the sensitivities from the combination of long-baseline and atmospheric neutrino data, the dashed curves correspond to long-baseline data only. We have assumed 10 years of data taking with a 440-kton detector.

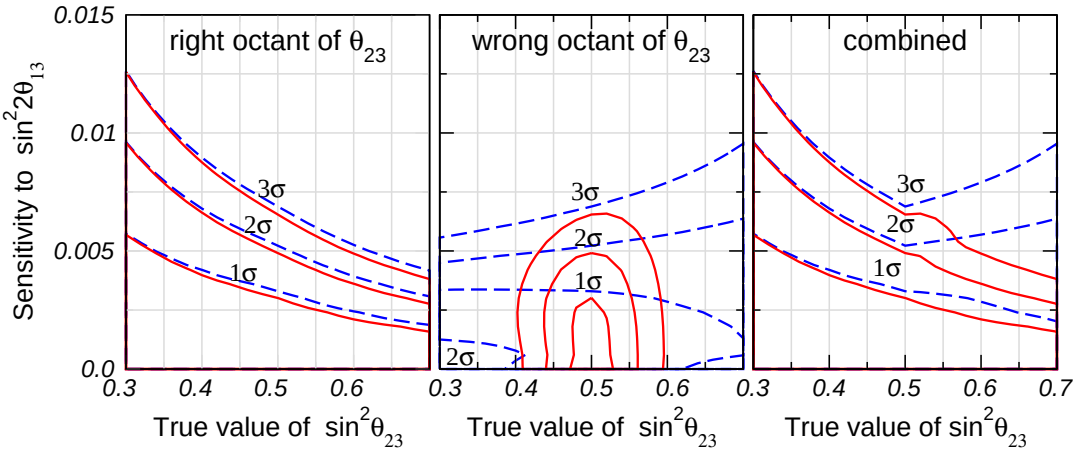

Figure 14: Sensitivity to $\sin^2 2\theta_{13}$ as a function of $\sin^2\theta_{23}^{\rm true}$ for LBL data only (dashed), and the combination LBL+ATM (solid). In the left and central panels we restrict the fit of θ_{23} to the octant corresponding to $\theta_{23}^{\rm true}$ and $\pi/2-\theta_{23}^{\rm true}$, respectively, whereas the right panel shows the overall sensitivity taking into account both octants. We have assumed 8 years of LBL and 9 years of ATM data taking with the T2HK beam and a 1 Mton detector.

the prompt e^+ and the delayed (200 μs) neutron capture produced by $\bar{\nu}_e + p \to n + e^+$ and emiting a 2.2 MeV photons. The energy window to look at the geo-neutrino events is $[1.7, 3.4]$ MeV: the lower bound corresponds to the reaction threshold while the upper bound is constraints by the nuclear reactor induced background events. The measured rate in the 1 kT liquid scintillator detector located at Kamioka (Japan) is 25^{+19}_{-18} for a total background of 127 ± 13 events. The background is composed by 2/3 of $\bar{\nu}_e$ from the nuclear reactors in Japan and Korea[6] and 1/3 of events coming from neutrons of 7.3 MeV produced in $^{13}{\rm C}(\alpha, n)^{16}{\rm O}$ reactions and captured as in the inverse beta decay reaction. The α particles come from the ^{210}Po decays daughter of the ^{222}Rn of natural radioactivity origin. The measured geo-neutrino events can be converted in a rate of $5.1^{+3.9}_{-3.6}\ 10^{-31}\ \bar{\nu}_e$ per target proton per year corresponding to a mean flux of 5.7 $10^6{\rm cm}^{-2}\ {\rm s}^{-1}$, or this can be transformed into a 99% CL upper bound of 1.45 $10^{-30}\ \bar{\nu}_e$ per target proton per year ($1.62\ 10^7{\rm cm}^{-2}\ {\rm s}^{-1}$ and 60 TW for the radiogenic power).

In MEMPHYS, one expects 10 times more geo-neutrino events but this would imply to decrease the trigger threshold to 2 MeV which seems challenging with respect to the present SuperKamiokande threshold set to 4.6 MeV due to high level of raw trigger rate 120 Hz and increasing by a factor 10 each times the trigger is lowered by 1 MeV [82]. This trigger rate is driven by a number of factors as γs from the rock surrounding the detector, radioactive decay in the PMT glass itself and Radon contamination in the water. So, it is a general interest to study in details the possibility to tackle the natural radioactivity of

[6] These events have been used by KamLAND to confirm and measure precisely the Solar driven neutrino oscillation parameters 3.8.

the detectors and their environment. To be confirmed by MEMPHYS

In LENA at the underground laboratory at CUPP a geo-neutrino rate of roughly 1000/y from the dominant $\bar{\nu}_e + p \rightarrow e^+ + n$ inverse beta-decay reaction is expected. The delayed coincidence measurement of the positron and the 2.2 MeV gamma event, following neutron capture on protons in the scintillator provides a very efficient tool to reject background events. The threshold energy of 1.8 MeV allows the measurement of geoneutrinos from the Uranium and Thorium series, but not from ^{40}K. We calculate for LENA at CUPP a reactor background rate of about 240 events per year in the relevant energy window from 1.8 MeV to 3.2 MeV. This background can be subtracted statistically using the information on the entire reactor neutrino spectrum up to $\simeq 8$ MeV. As it was shown in KamLAND a serious background source may come from radio impurities. There the correlated background from the isotope ^{210}Po is dominating. However, with an enhanced radiopurity of the scintillator, the background can be significantly reduced. Taking the radio purity levels of the CTF detector, where a ^{210}Po activity of $35 \pm 12/\mathrm{m}^3\mathrm{d}$ in PXE has been observed, this background would be reduced by a factor of about 150 compared to KamLAND and would account to less than 10 events per year in the LENA detector. An additional background that imitates the geoneutrino signal is due to ^{9}Li, which is produced by cosmic muons in spallation reactions with ^{12}C and decays in a β-neutron cascade. Only a small part of the ^{9}Li decays falls into the energy window which is relevant for geo-neutrinos. KamLAND estimates this background to be 0.30 ± 0.05 [81]. At CUPP the muon reaction rate would be reduced by a factor $\simeq 10$ due to better shielding and this background rate should be at the negligible level of $\simeq 1$ event per year in LENA.

From this considerations we follow that LENA would be a very capable detector for measuring geo-neutrinos. Different Earth's models could be tested with great significance. The sensitivity of LENA for probing the unorthodox idea of a geo-reactor in the Earth's core was estimated too. At the CUPP underground laboratory in Pyhäsalmi the neutrino background with energies up to $\simeq 8$ MeV due to nuclear power plants was calculated to be around 2200 events per year. At CUPP a 1 TW geo-reactor in the Earth's core would contribute 210 events per year and could be identified at a statistical level of better than 4σ after only one year of measurement and after 10 years a 4σ sensitivity for 0.3 TW would be reached.

Finally, in GLACIER the $\bar{\nu}_e + {}^{40}Ar \rightarrow e^+ + {}^{40}Cl^*$ has a threshold of 7.5 MeV which is too high for geo-neutrino detection.

3.6 Indirect Search for Dark Matter

WIMPs that constitute the halo of the Milky Way can occasionally interact with massive objects, such as stars or planets. When they scatter off of such an object, they can potentially lose enough energy that they become gravitationally bound and eventually will settle in the center of the celestial body. In particular, WIMPs can be captured by and accumulate in the core of the Sun.

We have assessed, in a model-independent way, the capabilities that GLACIER offers

for identifying neutrino signatures coming from the products of WIMP annihilations in the core of the Sun [83]. Signal events will consist of energetic electron (anti)neutrinos coming from the decay of τ leptons and b quarks produced in WIMP annihilation in the core of the Sun. Background contamination from atmospheric neutrinos is expected to be low. We do not consider the possibility of observing neutrinos from WIMPs accumulated in the Earth. Given the smaller mass of the Earth and the fact that only scalar interactions contribute, the capture rates for our planet are not enough to produce, in our experimental set-up, a statistically significant signal.

Our search method takes advantage of the excellent angular reconstruction and superb electron identification capabilities GLACIER offers to look for an excess of energetic electron (anti)neutrinos pointing in the direction of the Sun. The expected signal and background event rates have been evaluated, in a model independent way, as a function of the WIMP's elastic scatter cross section for a range of masses up to 100 GeV.

The detector discovery potential, i.e. the number of years needed to claim a WIMP signal has been discovered, is shown in Figs. 15 and 16. With the assumed set-up and thanks to the low background environment offered by the LAr TPC, a clear WIMP signal would be detected provided the elastic scattering cross section in the Sun is above $\sim 10^{-4}$ pb.

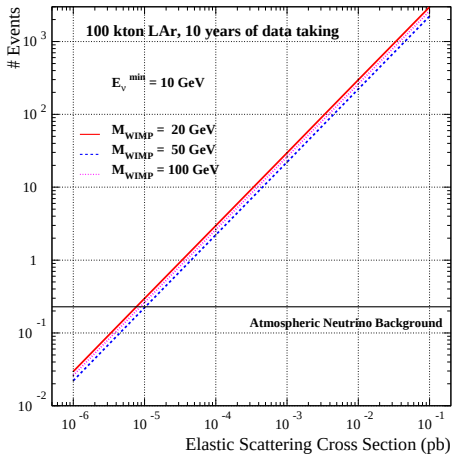

Figure 15: Expected number of signal and background events as a function of the WIMP elastic scattering production cross section in the Sun, with a cut of 10 GeV on the minimum neutrino energy.

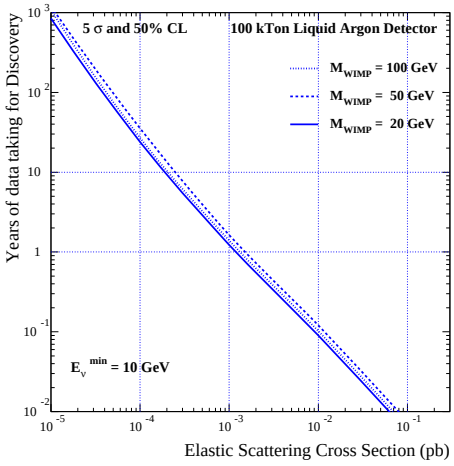

Figure 16: Minimum number of years required to claim a discovery WIMP signal from the Sun in a 100 kton LAr detector as function of σ_{elastic} for three values of the WIMP mass.

3.7 Neutrinos from reactors

It has been shown in sections 3.2 and 3.5 that $\bar{\nu}_e$ originated from nuclear reactors can be a serious background for diffuse supernova neutrino and geo-neutrino detections. But, a background on one side can be also turned to useful foreground on an other side. In particular, the KamLAND 1 kT liquid scintillator detector located at Kamioka had measured the flux of 53 Japanese power reactors delivering 701 Joule/cm^2 [84]. The event rate of 365.2 ± 23.7 above 2.6 MeV in 766 ton.y exposure from this nuclear power reactors was expected. The observed rate was 258 events with a total of background of 17.8 ± 7.3. The clear deficit interpreted in terms of neutrino oscillation leads to the measurement of θ_{12}, the neutrino 1-2 family mixing angle ($\sin^2\theta_{12} = 0.31^{+0.02}_{-0.03}$) as well as the mass squared difference $\Delta m^2_{12} = 7.9 \pm 0.3\ 10^{-5}\text{eV}^2$ (error quoted at 1 σ).

The area of precise measurement is now under investigation. Running KamLAND for 2-3 more years would gain 30% (4%) reduction in the spread of Δm^2_{12} (θ_{12}). It has been shown that using Water Čerenkov loaded with Gadolinium to increase by a factor 10 the neutron capture [85] one can expect 80% (34%) reduction of the spread of Δm^2_{12} (θ_{12}) in 110 kT.y exposure at Kamioka using SuperKamiokande.

Investigation of what could be expected using MEMPHYS loaded with Gadolinium and LENA is under investigation: waiting for the Th. Schwetz and S. Petcov letter.

A. Bueno comment: There have been no studies concerning the detection of reactor neutrinos with LAr TPC. I do not know whether this section is relevant or not, given the small amount of information we are able to give.

3.8 Neutrinos from beams

3.8.1 Introduction

In this section, we review the physics program offered by the proposed detectors using different accelerator based neutrino beams to push the search for non-zero θ_{13} value, or the measurement in case of previous discovery and the search for possible leptonic CP violation (δ_{CP}); to determine the mass hierarchy (i.e. the sign of Δm^2_{31}) and the θ_{23} octant (i.e. $\theta_{23} > 45°$ or $\theta_{23} < 45°$). We cover the potentiality of the so far studied MEMPHYS at Fréjus using a possible new CERN proton driver (SPL) to upgrade to 4MW the conventional neutrino beams (so-called Super Beams) and/or a possible new scheme of pure electron (anti)neutrino production by using radioactive ion decays (so-called βB Beam). Note that LENA is considered also as a candidate detector for the latter beam. Finally, as an ultimate tool, one thinks of producing very intense neutrino beams by mean of muon decays (so-called Neutrino Factory) that may be detected with a LAr detector as large as GLACIER.

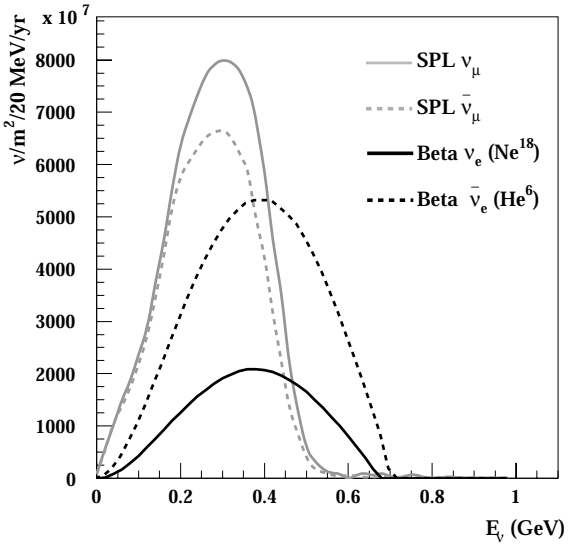

Figure 17: Neutrino flux of β-Beam ($\gamma = 100$) and CERN-SPL Super Beam, 3.5 GeV, at 130 km of distance (Fréjus).

3.8.2 The CERN-SPL Super Beam

The CERN-SPL Super Beam project is a conventional neutrino beam although based on a 4MW SPL (Superconducting Proton Linac) proton driver impinging a liquid mercury target to generate an intense π^+ (π^-) beam with small contamination of kaon mesons. The initial baseline [86, 87, 88, 89, 90] has been improved [91] considering the specific requirements of a CERN to Fréjus baseline (130 km). The SPL proton energy has been increased to 3.5 GeV/c and a new pion focusing system optimized. As a net effect the expected neutrino fluxes of the optimized version of the SPL beam line are shown on Fig. 17 and the event rates are presented in Tab. 9 for 2 years running with neutrinos and 8 years running with antineutrinos.

The use of a near and far detector will allow for both ν_μ disappearance and $\nu_\mu \to \nu_e$ appearance studies. The physics potential of the SPL Super Beam with MEMPHYS has been extensively studied [87, 89, 91, 93, 92]; however, the beam simulation will need some retuning after HARP results [94].

After 5 years exposure in ν_μ disappearance mode, a 3σ accuracy of (3-4)% can be acheived on Δm^2_{31}, and an accuracy of 22% (5%) on $\sin^2\theta_{23}$ if the true value is 0.5 (0.37) that is to say in case of a maximal mixing or a non-maximal mixing (Fig. 18). The use of atmospheric neutrinos (ATM) can alleviate the octant ambiguity in case of non-maximal mixing as it is shown in Fig. 18. Note however, thanks to a higher energy beam (~ 750 MeV), the T2HK project[7] can benefit from a much lower dependance on the Fermi

[7]Here, we make reference to the project where a 4MW proton driver may be build at KEK laboratory

	βB		SPL	
	$\delta_{\rm CP}=0$	$\delta_{\rm CP}=\pi/2$	$\delta_{\rm CP}=0$	$\delta_{\rm CP}=\pi/2$
appearance ν				
background	113		600	
$\sin^2 2\theta_{13}=0$	24		41	
$\sin^2 2\theta_{13}=10^{-3}$	66	76	93	10
$\sin^2 2\theta_{13}=10^{-2}$	285	314	387	126
appearance $\bar{\nu}$				
background	127		500	
$\sin^2 2\theta_{13}=0$	23		36	
$\sin^2 2\theta_{13}=10^{-3}$	64	10	74	104
$\sin^2 2\theta_{13}=10^{-2}$	271	100	297	390
disapp. ν	98178		21033	
background	5		1	
disapp. $\bar{\nu}$	72762		15731	
background	6		1	

Table 9: Number of events for appearance and disappearance signals and backgrounds for the βB, SPL to Fréjus scenario with MEMPHYS as far detector [92]. We have used 10 years of running in total for each beams. For the appearance signals the event numbers are given for several values of $\sin^2 2\theta_{13}$ and $\delta_{\rm CP}=0$ and $\pi/2$. The background as well as the disappearance event numbers correspond to $\theta_{13}=0$. For the other oscillation parameters the following values are used here and in the text as default values: $\Delta m^2_{31}=+2.4\times10^{-3}$ eV^2, $\sin^2\theta_{23}=0.5$, $\Delta m^2_{21}=7.9\times10^{-5}$ eV^2, $\sin^2\theta_{12}=0.3$.

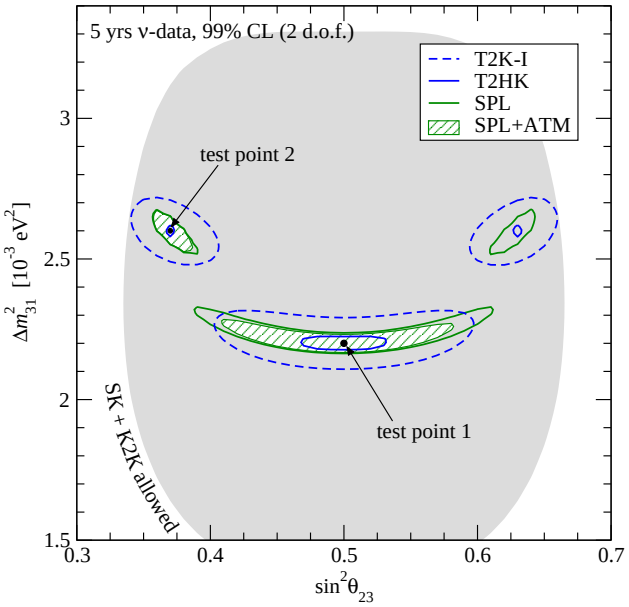

Figure 18: Allowed regions of Δm^2_{31} and $\sin^2\theta_{23}$ at 99% CL (2 d.o.f.) after 5 yrs of neutrino data taking for SPL, T2K phase I, T2HK, and the combination of SPL with 5 yrs of atmospheric neutrino data in the MEMPHYS detector. For the true parameter values we use $\Delta m^2_{31} = 2.2\,(2.6) \times 10^{-3}$ eV^2 and $\sin^2\theta_{23} = 0.5\,(0.37)$ for the test point 1 (2), and $\theta_{13} = 0$ and the solar parameters as: $\Delta m^2_{21} = 7.9 \times 10^{-5}$ eV^2, $\sin^2\theta_{12} = 0.3$. The shaded region corresponds to the 99% CL region from present SK and K2K data [95].

motion to obtain a better energy resolution and consequently better results.

In appearance mode (2 years ν_μ plus 8 years $\bar{\nu}_\mu$), a 3σ discovery of non-zero θ_{13}, irrespective of the actual true value of $\delta_{\rm CP}$, is achieved for $\sin^2 2\theta_{13} \gtrsim 4\ 10^{-3}$ ($\theta_{13} \gtrsim 3.6°$) as shown on Fig. 19. For maximal CP violation ($\delta^{\rm true}_{\rm CP} = \pi/2,\ 3\pi/2$) the same discovery level can be achieved for $\sin^2 2\theta_{13} \gtrsim 8\ 10^{-4}$ ($\theta_{13} \gtrsim 0.8°$). The best sensitivity for testing CP violation (i.e the data cannot be fitted with $\delta_{\rm CP} = 0$ nor $\delta_{\rm CP} = \pi$) is achieved for $\sin^2 2\theta_{13} \approx 10^{-2}$ ($\theta_{13} \approx 2.9°$) where 75% of the possible value of $\delta_{\rm CP}$ can be tested at 3σ (Fig. 20).

Although quite powerful, the SPL Super Beam is a conventional neutrino beam with known limitations due to 1) a lower production rate of anti-neutrinos compared to neutrinos which in addition to a smaller charged current cross-section impose to run 4 times longer in anti-neutrino modes; 2) the difficulty to setup a accurate beam simulation which implies to the design of a non-trivial near detector setup (cf. K2K, MINOS, T2K) to master the background level. Thus, a new type of neutrino beam, the so-called βB, is taken as a

to deliver an intense neutrino beam, which send to Kamioka mine is detected by a large Water Čerenkov detector.

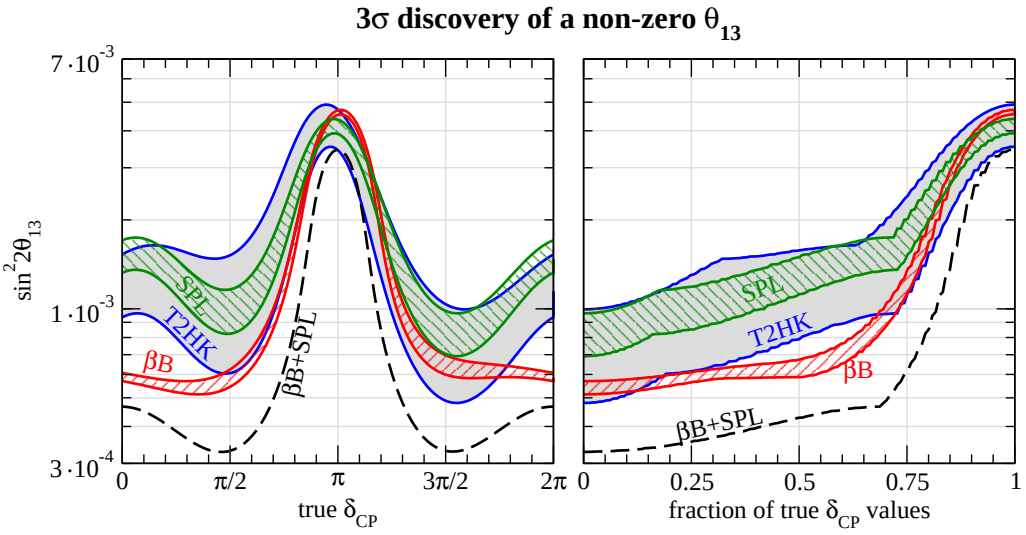

Figure 19: 3σ discovery sensitivity to $\sin^2 2\theta_{13}$ for βB, SPL, and T2HK as a function of the true value of $\delta_{\rm CP}$ (left panel) and as a function of the fraction of all possible values of $\delta_{\rm CP}$ (right panel). The width of the bands corresponds to values for the systematical errors between 2% and 5%. The dashed curves correspond to the combination of βB and SPL with 10 yrs of total data taking each for a systematical error of 2%.

attractive alternative and is described in the following section as well as a combination of the two kinds of beams.

3.8.3 The CERN-βB baseline scenario

Beta beams have been proposed by P. Zucchelli in 2001 [96]. The idea is to generate pure, well collimated and intense $\nu_e(\bar{\nu}_e)$ beams by producing, collecting, accelerating radioactive ions and storing them in a decay ring in 10 ns long bunches, to suppress the atmospheric neutrino backgrounds. The resulting βB spectra can be easily computed knowing the beta decay spectrum of the parent ion and the Lorentz boost factor γ, and these beams are virtually background free from other flavors. The best ion candidates so far are ^{18}Ne and ^{6}He for $\nu_e$and $\bar{\nu}_e$, respectively. A baseline study for the βB has been initiated at CERN, and is now going on within the European FP6 design study for EURISOL.

The potential of such βB sent to MEMPHYS has been studied in the context of the baseline scenario, using reference fluxes of $5.8{\cdot}10^{18}$ ^{6}He useful decays/year and $2.2{\cdot}10^{18}$ ^{18}Ne decays/year, corresponding to a reasonable estimate by experts in the field of the ultimately achievable fluxes. First oscillation physics studies [97, 98, 99, 100] used $\gamma_{^6\rm He} = 60$ and $\gamma_{^{18}\rm Ne} = 100$. But, it was soon realized that the optimal values were actually $\gamma = 100$ for both species, and the corresponding performances have been recently reviewed in reference [92].

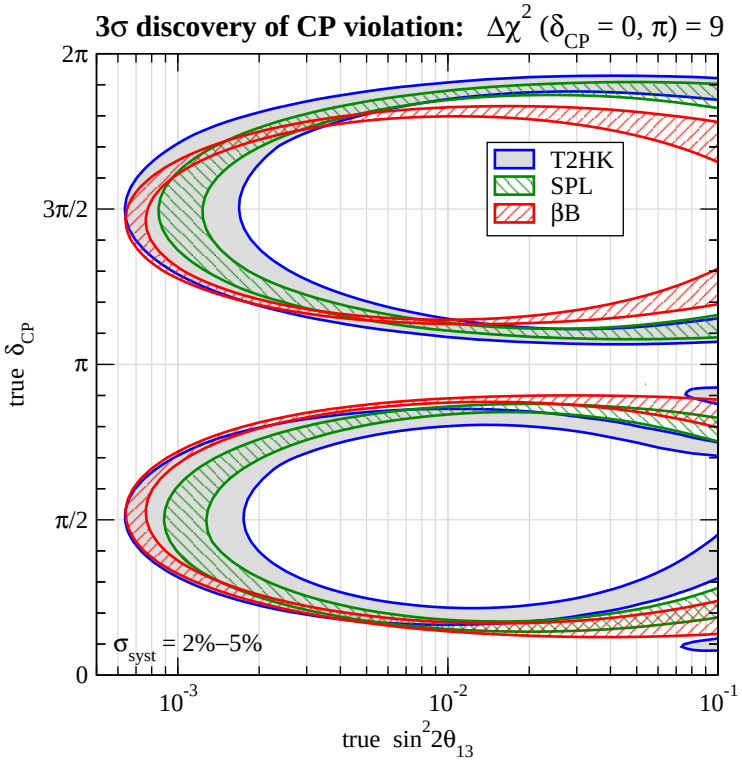

Figure 20: CPV discovery potential for βB, SPL, and T2HK: For parameter values inside the ellipse-shaped curves CP conserving values of $\delta_{\rm CP}$ can be excluded at 3σ ($\Delta\chi^2 > 9$). The width of the bands corresponds to values for the systematical errors from 2% to 5%.

On Fig. 19 the result of running a βB during 10 years (5 years with neutrinos and 5 years with anti-neutrinos) is shown and prove to be better compared to a SPL Super beam run, especially for maximal CP violation where a non-zero θ_{13} value can be stated at 3σ for $\sin^2 2\theta_{13} \gtrsim 6\ 10^{-3}$ ($\theta_{13} \gtrsim 2.2°$). Moreover, it is noticeable (Figs. 19,20) that the βB is less affected by systematic errors on the background compared to the SPL Super beam and T2HK.

Before combining the two possible CERN beams, let us consider LENA as potential detector. LENA (Comment by JEC: which mass?) can as well be used as detector for a low-energy βB oscillation experiment. Using a neutrino beam of about 600-800 MeV, muon events are separable from electron events due to their different track lengths in the detector and due to the electron emitted in the muon decay after a mean time of 2.2 μs.

In simulations it has been shown that for those energies, muons travel $\sim$ 3 m while electrons only $\sim$ 1 m as electrons undergo scattering and bremsstrahlung. This results in different distributions of the number of photons and the timing pattern, which can be used to distinguish between the two classes of events. Further studies on the event position reconstruction will be performed to estimate the efficiency of muon/electron separation. In addition, muons can be recognized by observing the electron of its succeeding decay. It has been calculated that the efficiency in the detection of these electrons is $\sim$ 96%. For the rest of events the decay happens too fast and cannot be resolved from the preceding muon signal.

It is important to point out that for the mentioned muon/electron separation, a fiducial volume has to be defined to guarantee full contained events. This would reduce the fiducial volume of LENA by only 10%.

The advantage of using a liquid scintillator detector for such an experiment is the good energy reconstruction of the neutrino beam. Neutrinos of these energies can produce delta resonances which subsequently decay into nucleon and pion. In Water Čerenkov detectors, pions with energies under the Čerenkov threshold contribute to the error in the energy of the neutrino. In LENA these particles can be detected.

To conclude this section, let us mention a very recent development of the βB concept: first, authors of reference [101] are considering a very promising alternative for the production of ions, and secondly, the possibility to have monochromatic, single flavor neutrino beams by using ions decaying through the electron capture process [102, 103]. Such beams would in particular be perfect to precisely measure neutrino cross sections in a near detector with the possibility of an energy scan by varying the γ value of the ions.

3.8.4 combining SPL Beam and βB with MEMPHYS at Fréjus

Since a βB uses only a small fraction of the protons available from the SPL, Super and Beta beams can be run at the same time. Their combination leads to further improvements on the sensitivity on θ_{13} and $\delta_{\rm CP}$, as shown on Fig. 19. It pushes especially at maximal CP violation the discovery potential down to $\sin^2 2\theta_{13} \gtrsim 3\ 10^{-4}$ ($\theta_{13} \gtrsim 0.5°$).

Moreover, using only neutrino modes, ν_μ for SPL and ν_e for βB, if CPT symmetry is

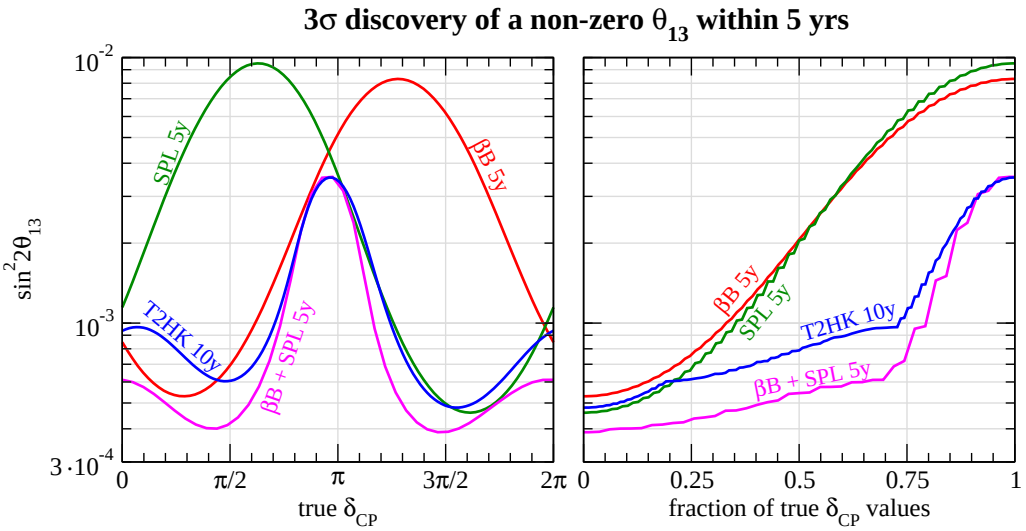

Figure 21: Discovery potential of a finite value of $\sin^2 2\theta_{13}$ at 3σ ($\Delta\chi^2 > 9$) for 5 yrs neutrino data from βB, SPL, and the combination of βB + SPL compared to 10 yrs data from T2HK (2 yrs neutrinos + 8 yrs antineutrinos).

assumed, all the information can be obtained as $P_{\bar{\nu}_e\to\bar{\nu}_\mu} = P_{\nu_\mu\to\nu_e}$ and $P_{\bar{\nu}_\mu\to\bar{\nu}_e} = P_{\nu_e\to\nu_\mu}$. We illustrate this synergy in Fig. 21. In this scenario, time consuming anti-neutrino running can be avoided keeping the same physics discovery potential.

One can also combine SPL, βB and the atmospheric neutrinos (ATM) to alleviate the parameter degeneracies which lead to disconnected regions on the multi-dimensional space of oscillation parameters[8]. Atmospheric neutrinos, mainly multi-GeV e-like events, are sensitive to the neutrino mass hierarchy if θ_{13} is sufficiently large due to Earth matter effects, whilst sub-GeV e-like events provide sensitivity to the octant of θ_{23} due to oscillations with Δm^2_{21}.

The result of running during 5 years on neutrino mode for SPL and βB, adding further the ATM data, is shown on Fig. 22 [92]. One can appreciate that practically all the degeneracies can be eliminated as only the solution with the wrong sign survives with a $\Delta\chi^2 = 3.3$. This last degeneracy can be completely eliminated using neutrino mode combined with anti-neutrino mode and ATM data [92], however the example shown is a favorable case with $\sin^2\theta_{23} = 0.6$, and in general for $\sin^2\theta_{23} < 0.5$ the impact of the atmospheric data is weaker.

So, as a generic case, for the CERN-MEMPHYS project, one is left with the four intrinsic degeneracies. However, the important observation of Fig. 22 is that degeneracies have only a very small impact on the CP violation discovery, in the sense that if the true solution is CP violating also the fake solutions are located at CP violating values of $\delta_{\rm CP}$.

[8] See reference [104] for the definitions of *intrinsic*, *hierarchy*, and *octant* degeneracies

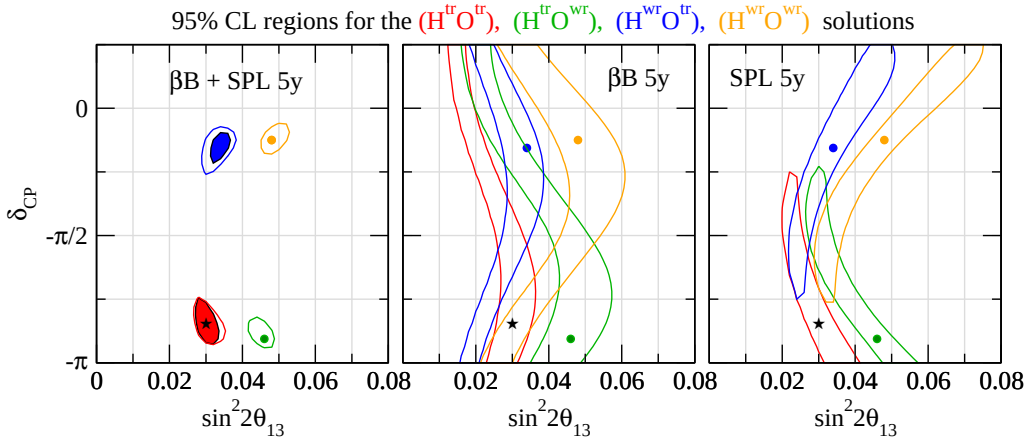

Figure 22: Allowed regions in $\sin^2 2\theta_{13}$ and $\delta_{\rm CP}$ for 5 years data (neutrinos only) from βB, SPL, and the combination. $\mathrm{H}^{\rm tr/wr}(\mathrm{O}^{\rm tr/wr})$ refers to solutions with the true/wrong mass hierarchy (octant of θ_{23}). For the colored regions in the left panel also 5 years of atmospheric data are included; the solution with the wrong hierarchy has $\Delta\chi^2 = 3.3$. The true parameter values are $\delta_{\rm CP} = -0.85\pi$, $\sin^2 2\theta_{13} = 0.03$, $\sin^2\theta_{23} = 0.6$. For the βB only analysis (middle panel) an external accuracy of 2% (3%) for $|\Delta m^2_{31}|$ (θ_{23}) has been assumed, whereas for the left and right panel the default value of 10% has been used.

Therefore, thanks to the relatively short baseline without matter effect, even if degeneracies affect the precise determination of θ_{13} and $\delta_{\rm CP}$, they have only a small impact on the CP violation discovery potential. Furthermore, one would quote explicitly the four possible set of parameters with their respective confidential level. It is also clear from the figure that the sign(Δm^2_{31}) degeneracy has practically no effect on the θ_{13} measurement, whereas the octant degeneracy has very little impact on the determination of $\delta_{\rm CP}$.

Another feature of the ATM data is to provide a non-trivial sensitivity to the neutrino mass hierarchy (i.e. the sign of Δm^2_{31}) as shown on Fig. 23 for 10 years run. The mass hierarchy can be identified at 2σ CL provided $\sin^2 2\theta_{13} \gtrsim 0.02$ for βB and SPL combined [92].

Finally, before ending this section, it may be worth mentioning that the combination of Super and β beams offers advantages, from the experimental point of view, since the same parameters θ_{13} and δ_{CP} may be measured in many different ways, using 2 pairs of CP related channels, 2 pairs of T related channels, and 2 pairs of CPT related channels which should all give coherent results. In this way the estimates of the systematic errors, different for each beam, will be experimentally cross-checked. And, needless to say, the unoscillated data for a given beam will give a large sample of events corresponding to the small searched-for signal with the other beam, adding more handles on the understanding of the detector response.

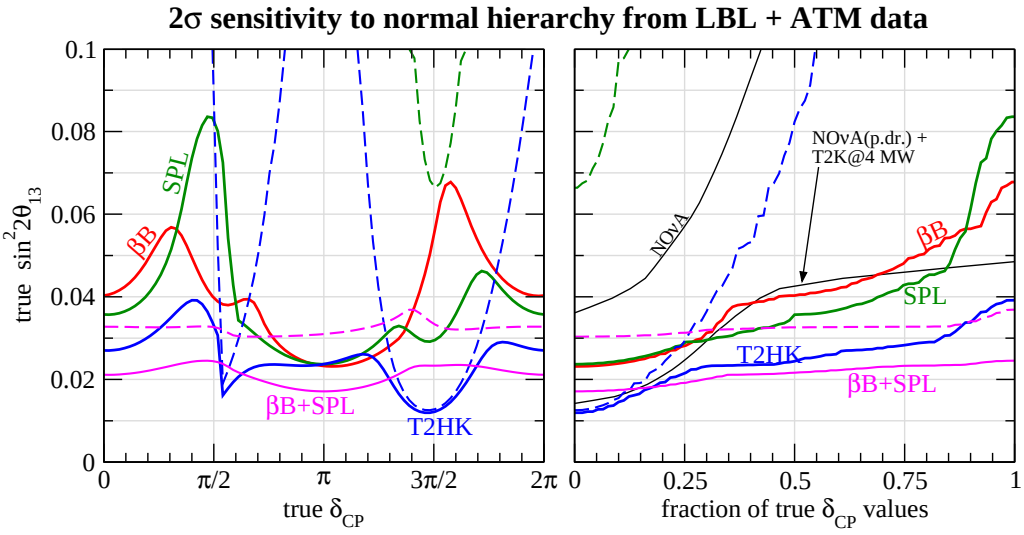

Figure 23: Sensitivity to the mass hierarchy at 2σ ($\Delta\chi^2 = 4$) as a function of the true values of $\sin^2 2\theta_{13}$ and $\delta_{\rm CP}$ (left), and the fraction of true values of $\delta_{\rm CP}$ (right). The solid curves are the sensitivities from the combination of long-baseline and atmospheric neutrino data, the dashed curves correspond to long-baseline data only. For comparison we show in the right panel also the sensitivities of NOνA and NOνA+T2K extracted from Fig. 13.14 of Ref. [78]. For the curve labeled "NOνA (p.dr.)+T2K@4 MW" a proton driver has been assumed for NOνA and the T2K beam has been up-graded to 4 MW, see Ref. [78] for details.

3.8.5 Neutrino Factory LAr detector

In order to fully address the oscillation processes at a neutrino factory, a detector should be capable of identifying and measuring all three charged lepton flavors produced in charged current interactions *and* of measuring their charges to discriminate the incoming neutrino helicity. This is an experimentally challenging task, given the required detector mass for long-baseline experiments.

The GLACIER concept offers a high granularity, excellent calorimetry non magnetized target detector, which provides a background free identification of electron neutrino charged current and a kinematical selection of tau neutrino charged current interactions. We can assume that charge discrimination is available for muons reaching an external magnetized-Fe spectrometer. Another interesting and extremely challenging possibility would consist on magnetizing the whole liquid argon volume [112]. This set-up allows the clean classification of events into electron, right-sign muon, wrong-sign muon and no-lepton categories. In addition, high granularity permits a clean detection of quasi-elastic events, which by detecting the final state proton, provide a selection of the neutrino electron helicity without the need of an electron charge measurement.

Table 10 summarizes the expected rates for GLACIER and 10^{20} muon decays (expected 1 year of operation) at a neutrino factory with stored muons having an energy of 30 GeV [113]. N_{tot} is the total number of events and N_{qe} is the number of quasi-elastic events.

Event rates for various baselines							
		L=732 km		L=2900 km		L=7400 km	
		N_{tot}	N_{qe}	N_{tot}	N_{qe}	N_{tot}	N_{qe}
	ν_μ CC	2260000	90400	144000	5760	22700	900
μ^-	ν_μ NC	673000	–	41200	–	6800	–
10^{20} decays	$\overline{\nu}_e$ CC	871000	34800	55300	2200	8750	350
	$\overline{\nu}_e$ NC	302000	–	19900	–	3000	–
	$\overline{\nu}_\mu$ CC	1010000	40400	63800	2550	10000	400
μ^+	$\overline{\nu}_\mu$ NC	353000	–	22400	–	3500	–
10^{20} decays	ν_e CC	1970000	78800	129000	5160	19800	800
	ν_e NC	579000	–	36700	–	5800	–

Table 10: Expected events rates for the GLACIER detector in case no oscillations occur for 10^{20} muon decays. We assume E_μ=30 GeV. N_{tot} is the total number of events and N_{qe} is the number of quasi-elastic events.

Figure 24 shows the expected sensitivity in the measurement of the mixing angle between the first and the third family for a baseline of 7400 km. The maximal sensitivity to θ_{13} is achieved for very small background levels, since we are looking in this case for small signals; most of the information is coming from the clean wrong-sign muon class and from

quasi-elastic events. On the other hand, if its value is not too small, for a measurement of θ_{13}, the signal/background ratio could be not so crucial, and also the other event classes can contribute to this measurement.

Like for a B-Factory, a ν-Factory should have among its aims the over constraining of the oscillation pattern, in order to look for unexpected new physics effects. This can be achieved in global fits of the parameters, where the unitarity of the mixing matrix is not strictly assumed. Using a detector able to identify the τ lepton production via kinematic means, it is possible to verify the unitarity in $\nu_\mu \rightarrow \nu_\tau$ and $\nu_e \rightarrow \nu_\tau$ transitions. For this latter, the possibility of a kinematical τ identification for wrong-sign muon events could allow for the first time a clear identification of this type of oscillations.

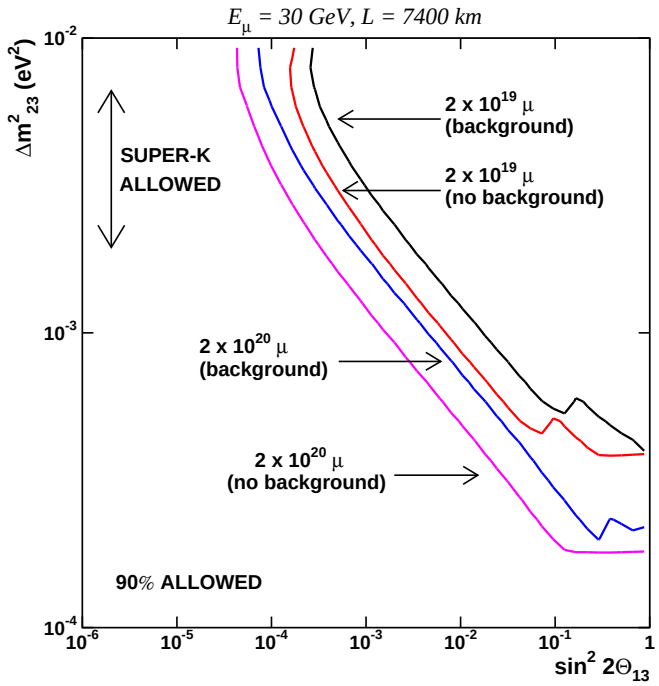

Figure 24: GLACIER sensitivity for θ_{13}.

The study of CP violation in the lepton system is a very fascinating subject and probably, the most ambitious goal of an experiment at a neutrino factory. Matter effect can mimic CP violation; however, a multi parameter fit at the right baseline can allow a simultaneous determination of matter and CP-violating parameters.

To detect CP violation effects, the most favorable choice of neutrino energy E_ν and baseline L is in the region of the "first maximum", given by $(L/E_\nu)^{max} \simeq 500$ km/GeV for $|\Delta m^2_{32}| = 2.5 \times 10^{-3}$ eV^2 [114]. To study oscillations in this region, one has to require that the energy of the "first-maximum" be smaller than the MSW resonance energy:

$2\sqrt{2}G_F n_e E_\nu^{max} \lesssim \Delta m^2_{32} \cos 2\theta_{13}$. This fixes a limit on the baseline L_{max} ≈5000 km beyond which matter effects spoil the sensitivity.

As an example, Fig. 25 shows the sensitivity on the CP violating phase δ for two concrete cases. We have classified the events in the five categories previously mentioned, assuming an electron charge confusion of 0.1%. We have computed the exclusion regions in the $\Delta m^2_{12} - \delta$ plane fitting the visible energy distributions, provided that the electron detection efficiency is $\sim 20\%$. The excluded regions extend up to values of $|\delta|$ close to π, even when θ_{13} is left free.

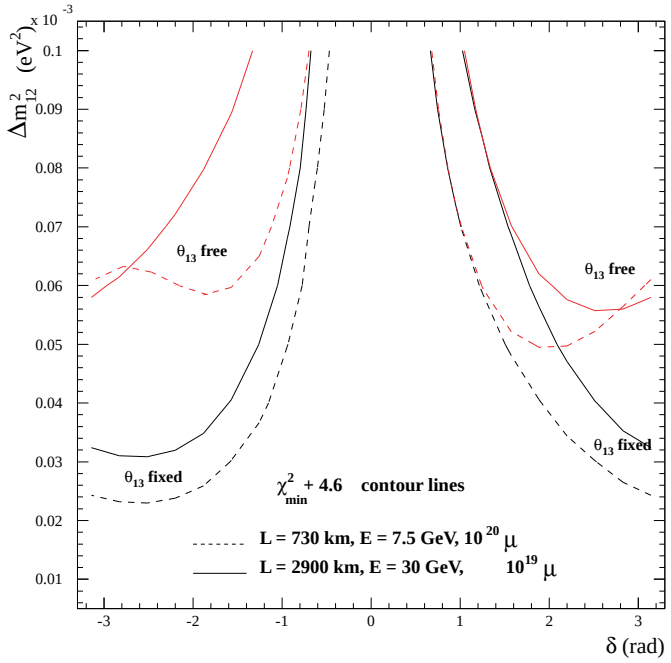

Figure 25: GLACIER 90% C.L. sensitivity on the CP-phase δ as a function of Δm^2_{21} for the two considered baselines. The reference oscillation parameters are $\Delta m^2_{32} = 3 \times 10^{-3}$ eV^2, $\sin^2\theta_{23} = 0.5$, $\sin^2\theta_{12} = 0.5$, $\sin^2 2\theta_{13} = 0.05$ and $\delta = 0$. The lower curves are made fixing all parameters to the reference values while for the upper curves θ_{13} is free.

4 Underground sites

The proposed large detectors require underground site naturally protected against cosmic rays that induce background events mainly for non-accelerator type of physics. Other

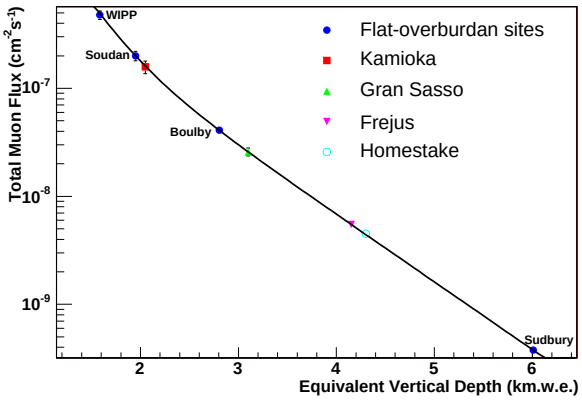

Figure 26: The total muon flux measured for the various underground sites as a function of the equivalent vertical depth relative to a flat overburden. The smooth curve is a global fit function to those data taken from sites with flat overburden (equation 7) [115].

considerations take place as the accessibility to the experiment, the possibility to proceed to large excavation at reasonable cost and time... One of the main objectives of the ILIAS European Joint Research Activity Network is to identify and measure the different background components of experiments carried out in the underground laboratories, and to design methods and techniques to suppress them. Some measurements are still underway and all underground sites are not at the same level of qualification.

Nevertheless in Tab. 11 some background characteristics are summarized for the underground laboratories that might host the proposed detectors. In this table the equivalent depth is defined according to reference [115] to the depth where the same muon intensity occurs for a flat overburden laboratory. In this case the muon flux I_μ (cm^{-2}s^{-1}) at a given depth h_e (km.w.e) has been adjusted and it yields (Fig. 26):

$$I_\mu(h_e) = \left(67.97e^{-h_e/0.285} + 2.071e^{-h_e/0.698}\right) \times 10^{-6} \tag{7}$$

Using the same equivalent depth, the muon-induced neutron flux (cm^{-2}s^{-1}) emerging from the rock can also be parametrized as

$$I_n(h_e) = \left[(4.0 \pm 1.1)\frac{0.86 \pm 0.05}{h_e}e^{-h_e/(0.86\pm0.05)}\right] \times 10^{-7} \tag{8}$$

and is shown on Fig. 27. In the following sections more details on the sites are given.

4.1 Fréjus location

The site located in the Fréjus mountain in the Alps, which is crossed by a road-tunnel connecting France (Modane) to Italy (Bardonecchia), has a number of interesting charac-

	Fréjus	Pyhäsalmi	Boulby	Canfranc	Sieroszowice
Location	Italy-France border	Finland	UK	Spain	Poland
Type	Fréjus tunnel	Mine	Potash Mine	Somport tunnel	Mine
Vertical Depth (km.w.e)	4.8	4.0	3.5 ?	2.5	?
Equiv. Depth (km.w.e)	4.2	?	2.8	?	?
μ Flux (10^{-9} cm^{-2}s^{-1})	4.8	?	41.7	200.0	?
n Flux (10^{-6} cm^{-2}s^{-1})	1.6 (0-0.63 eV) 4.0 (2-6 MeV)	?	2.8 (>100 keV) 1.3 (>1 MeV)	3.82 (integral)	?
γ Flux (cm^{-2}s^{-1})	7.0 (>4 MeV)	?	?	2 10^{-2} (energy?)	?
^{238}U (ppm) Rock/Cavern	0.84/1.90	28-44 Bq/m^3	0.07	30 Bq/kg	?
^{232}Th (ppm) Rock/Cavern	2.45/1.40	4-19 Bq/m^3	0.12	76 Bq/kg	?
K (Bq/kg) Rock/Cavern	213/77	267-625 Bq/m^3	1130	680	?
Rn (Bq/m^3) Cavern (Vent. ON/OFF)	15-150	10-148 ?	?	50-100 Bq/kg	?

Table 11: Summary of relevant characteristics of some sites foreseen for the proposed detectors. The Rn content depends on the ventilation of the cavity. To be completed and cross-checked and unit uniformized as possible.

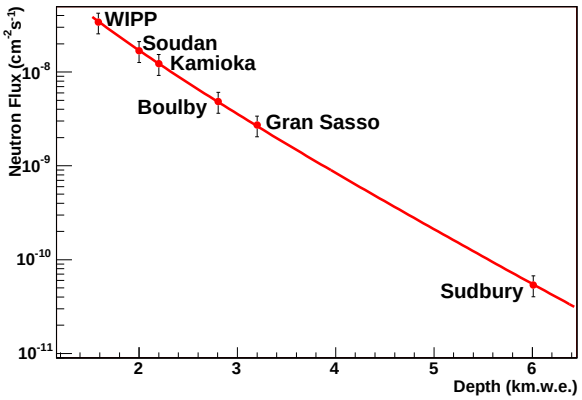

Figure 27: The total muon-induced neutron flux deduced for the various underground sites displayed with the parametrization of equation 8 [115].

teristics making it a very good candidate for the installation of a megaton-scale detector in Europe, aimed both at non-accelerator and accelerator based physics. Its great depth, the good quality of the rock, the fact that it offers horizontal access, its distance from CERN (130 km), the opportunity of the excavation of a second ("safety") tunnel, the very easy access by train (TGV), by car (highways) and by plane (Geneva, Torino and Lyon airports), the strong support from the local authorities represent the most important of these characteristics.

On the basis of these arguments, the DSM (CEA) and IN2P3 (CNRS) institutions decided to perform a feasibility study of a Large Underground Laboratory in the central region of the Fréjus tunnel, near the already existing, but much smaller, LSM Laboratory. This preliminary study has been performed by the SETEC (French) and STONE (Italian) companies and is now completed. These companies already made the study and managed the realisation of the Fréjus road tunnel and of the LSM (Laboratoire Souterain de Modane) Laboratory. A large number of precise and systematic measurements of the rock characteristics, performed at that time, have been used to make a pre-selection of the most favorable regions along the road tunnel and to constrain the simulations of the present pre-study for the Large Laboratory.

Three regions have been pre-selected : the central region and two other regions at about 3 km from each entrance of the tunnel. Two different shapes have been considered for the cavities to be excavated: the "tunnel shape" and the "shaft shape" and the main purpose was to determine the maximum possible size for each of them, the most sensitive dimension being the width (the so-called "span") of the cavities.

The very interesting results of this preliminary study can be summarized as follows :

1. the best site (rock quality) is found in the middle of the mountain, at a depth of

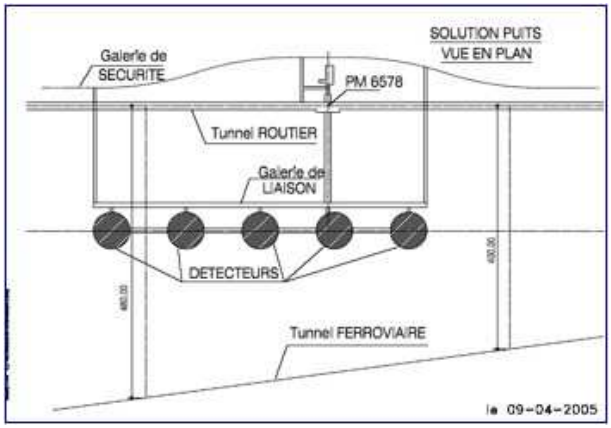

Figure 28: Envisaged configuration of the Fréjus underground laboratory.

4800 m.w.e (vertical depth);

2. of the two considered shapes : "tunnel" and "shaft", the "shaft shape" is strongly preferred;

3. cylindrical shafts are feasible up to a diameter $\Phi = 65$ m and a full height $h = 80$ m (~ 250000 m^3) (see Fig. 29 as an example);

4. with "egg shape" or "intermediate shape between cylinder and egg shapes" the volume of the shafts could be still increased;

5. the estimated cost is ~ 80 M€ per shaft. JEC comment: should we put this kind of cost estimate ?

Fig. 28 shows a possible configuration for this large Laboratory, where up to five shafts, of about 250000 m^3 each, can be located between the road tunnel and the railway tunnel, in the central region of the Fréjus mountain.

Two possible scenarios for Water Čerenkov detectors are, for instance:

- 3 shafts of 250000 m^3 each, with a fiducial mass of 440 kton ("UNO-like" scenario).
- 4 shafts of 250000 m^3 each, with a fiducial mass of 580 kton.

In both scenarios one additional shaft could be excavated for a Liquid Argon of about 100 kton total mass.

4.2 Pyhäsalmi location

The Pyhäsalmi mine is located in Pyhäjärvi which is a small town in the central Finland. The mine is the deepest base-metal mine in Europe, extending at the moment down to

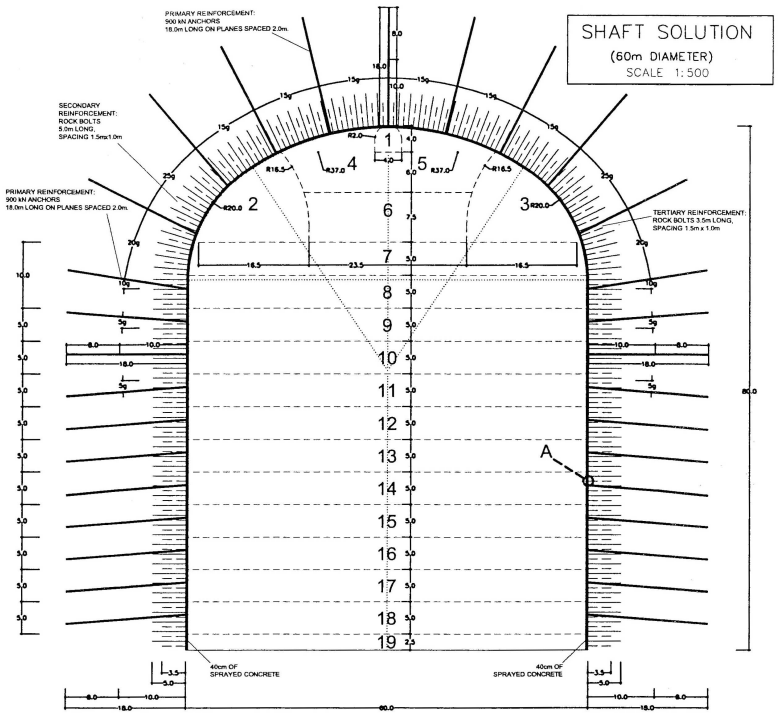

Figure 29: An example of "shaft shape" simulation, constrained by the rock parameter measurements made during the road tunnel and the present laboratory excavation. As a rule of thumb, the main feasibility criterion is that the significantly perturbed region around the cavity should not exceed a thickness of about 10 m which is about half of the length of the longuest anchors shown.

1440 metres, corresponding to about 4000 m.w.e. It is run by Pyhäsalmi Mine Ltd and owned by Inmet Mining Corporation, Canada. The mine is active, producing copper and zinc, and the estimated ore capacity is until 2016 at the moment.

The site provides modern infrastructures and very good traffic conditions all around a year. This includes a railway line apt for heavy transport.

The northern location is very beneficial for neutrino studies. There are not many nuclear reactors around and therefore the reactor neutrino background is small which allows studies of geoneutrinos and diffuse supernova neutrino background. To observe Earth matter effects for galactic supernova neutrinos Pyhäsalmi provides a possibility of 58% that the neutrinos pass through the core, compared with 60% in the North Pole. The distance to CERN is 2288 km which is very interesting for neutrino beam studies.

The mine can be divided into the old and new parts. The old mine goes down to 1050 metres (3000 m.w.e) and the new mine is directly below it. Major parts of the old mine are free for experiments and there are several caverns to be used, also large ones. In the new mine small-scale experiments could be constructed out at the moment, the largest scale being about 10 m $\times$ 10 m $\times$ 10 m. Larger excavations come possible in the future when the mining activities cease in those parts.

A prefeasibility study indicated that the excavation of large-scale caverns is technically possible. The largest cavern studied in detail was 20 m $\times$ 20 m $\times$ 120 m, but that is by no means an upper limit for the size. The Finnish bedrock consists of very hard and old crystalline rock, which is the very best for construction of large volume cavities. For example, numerous underground oil and gas storage tanks have been built in Finland at the depths of some tens to some hundred metres, with a total volume larger than 10,000,000 m^3, the largest individual tank being 2,000,000 m^3. Even though the tanks are not armored at all and only the solidness of the rock and the pressure of the ground water protect the fuel from escaping, no leakages to environment have been observed.

The laboratory is taking the first steps toward larger-scale experiments. A cosmic-ray experiment EMMA is starting to collect data during 2006 at the shallow depth. A supernova neutrino experiment is planned to be constructed in few years at the old part of the mine. The prototype detector of a large liquid scintillator (LENA) is also anticipated to be built in the near future at the depth of 1410 metres.

5 Summary

The three proposed detectors (MEMPHYS, LENA, GLACIER) based on completely different detection techniques (Water Čerenkov, Liquid Scintillator, Liquid Argon) share to a large extent a very rich physics program and in some cases their detection specificities are complementary. A brief summary of the scientific case is presented both for non-accelerator based topics and the accelerator neutrino oscillation topic on tables 12 and 13, respectively.

Topics	**GLACIER** (100 kt)	**LENA** (50 kt)	**MEMPHYS** (440 kt)
Proton decay			
$e^+\pi^0$	0.5×10^{35}	-	1.0×10^{35}
$\bar{\nu}K^+$	1.1×10^{35}	0.4×10^{35}	0.2×10^{35}
SN ν (10 kpc)			
CC	2.5 $10^4(\nu_e)$	9.0 $10^3(\bar{\nu}_e)$	2.0 $10^5(\bar{\nu}_e)$
NC	3.0 10^4	3.0 10^3	-
ES	1.0 $10^3(e)$	7.0 $10^3(p)$	1.0 $10^3(e)$
DSN ν (5 yrs Sig./Bkgd)	?-60/30	10-115/4	43-109/47 (*)
Solar ν (1 yr Sig.)	4.5 10^4/1.6 10^5 (^{8}B ES/Abs)	2.0 10^6/7.7 10^4/360 (^{7}Be/*pep*/^{8}B)	1.1 10^5 (^{8}B ES)
Atmospheric ν (1 yr Sig.)	1.1 10^4	?	4.0 10^4 (1-ring only)
Geo ν (1 yr Sig.)	below threshold	≈ 1000	need 2 MeV threshold
Reactor ν (1 yr Sig.)	?	1.7 10^4	6.0 10^4 (*)
Dark Matter 10 yrs Sig.	3 events ($\sigma_{ES} = 10^{-4}$,$M > 20$ GeV)	?	?

Table 12: Brief summary of the physics potential of the proposed detectors for non-accelerator based topics. The (*) stands for the case where one MEMPHYS shaft is filled with Gadolinium.To be completed

Detector	Beam type	Running time	Potentialities
MEMPHYS	CERN-SPL (disapp.)	5 yrs	$\delta\Delta m^2_{31} = (3-4)\%$ and $\delta \sin^2\theta_{23} = (5-22)\%$
	CERN-SPL (app.)	10 yrs	$\theta_{13}^{3\sigma} \approx 1.8^\circ$ ($\delta_{\rm CP} = 0, \pi$) and $\theta_{13}^{3\sigma} \approx 0.8^\circ$ ($\delta_{\rm CP} = \frac{\pi}{2}, \frac{3\pi}{2}$)
	CERN-βB (app.)	10 yrs	$\theta_{13}^{3\sigma} \approx 1.9^\circ$ ($\delta_{\rm CP} = 0, \pi$) and $\theta_{13}^{3\sigma} \approx 0.7^\circ$ ($\delta_{\rm CP} = \frac{\pi}{2}, \frac{3\pi}{2}$)
	SPL+βB (app.)	5 yrs	$\theta_{13}^{3\sigma} \approx 1.7^\circ$ ($\delta_{\rm CP} = 0, \pi$) and $\theta_{13}^{3\sigma} \approx 0.6^\circ$ ($\delta_{\rm CP} = \frac{\pi}{2}, \frac{3\pi}{2}$)
	SPL+βB (app.)	10 yrs	$\theta_{13}^{3\sigma} \approx 1.7^\circ$ ($\delta_{\rm CP} = 0, \pi$) and $\theta_{13}^{3\sigma} \approx 0.5^\circ$ ($\delta_{\rm CP} = \frac{\pi}{2}, \frac{3\pi}{2}$) 75% of all $\delta_{\rm CP}$ at 3σ for $\theta_{13} = 3^\circ$
	SPL+βB+ATM	10 yrs	2σ mass hier. for $\theta_{13} > 4^\circ$, degeneracy reduction
GLACIER			

Table 13: Brief summary of the physics potential of the proposed detectors for accelerator oscillation topic. To be completed

Acknowledgments

To be completed: P.F. Perez, A. Mirizzi

References

[1] K. Hirata *et al.* [KAMIOKANDE-II Collaboration], Phys. Rev. Lett. **58**, 1490 (1987).

[2] K. S. Hirata *et al.*, Phys. Rev. D **38**, 448 (1988).

[3] M. Aglietta et al. , Europhys. Lett. 3 (1987) 1321

[4] R. M. Bionta *et al.*, Phys. Rev. Lett. **58**, 1494 (1987).

[5] K.S. Hirata et al. , *Phys. Rev. Lett.* 63 (1989) 16

[6] K. S. Hirata et al. , *Phys. Lett.* B 205 (1988) 416

[7] Y. Fukuda et al. , *Phys. Rev. Lett.* 81 (1998) 1562

[8] E. Aliu et al. , *Phys. Rev. Lett.* 94 (2005) 081802

[9] A. Rubbia, hep-ph/0402110, hep-ph/0407297; A. Ereditatio, A. Rubbia, hep-ph/0409143.

[10] Oberauer L, von Feilitzsch F, and Potzel W 2005 *Nucl. Phys.* B *(Proc. Suppl.)* **138** 108

[11] Marrodán Undagoitia T et al. 2005 *Phys. Rev.* D **72** 075014 *(Preprint hep-ph/0511230)*

[12] A. de Bellefon et al., MEMPHYS: A large scale water Čerenkov detector at Fréjus, Contribution to the CERN strategic committee

[13] S. Amerio *et al.* [ICARUS Collaboration], Nucl. Instrum. Meth. A **527**, 329 (2004).

[14] Schoenert S et al. (BOREXINO Collaboration) 2004 *(Preprint physics/0408032)*

[15] M. Wurm, Diploma thesis 2005

[16] To be defined

[17] Beacom, J. F. and Vagins, M. R., *Phys. Rev. Lett.* 93 (2004) 171101, arXiv:hep-ph/0309300

[18] P. Nath and P. Fileviez Pérez, "Proton stability in grand unified theories, in strings, and in branes," arXiv:hep-ph/0601023. Submitted to Physics Reports.

[19] I. Dorsner and P. Fileviez Pérez, "How long could we live?," Phys. Lett. B **625** (2005) 88 [arXiv:hep-ph/0410198].

[20] H. Georgi and S. L. Glashow, "Unity Of All Elementary Particle Forces," Phys. Rev. Lett. **32** (1974) 438.

[21] I. Dorsner and P. Fileviez Pérez, "Unification without supersymmetry: Neutrino mass, proton decay and light leptoquarks," Nucl. Phys. B **723** (2005) 53 [arXiv:hep-ph/0504276]; I. Dorsner, P. Fileviez Pérez and R. Gonzalez Felipe, "Phenomenological and cosmological aspects of a minimal GUT scenario," arXiv:hep-ph/0512068.

[22] D. G. Lee, R. N. Mohapatra, M. K. Parida and M. Rani, "Predictions for proton lifetime in minimal nonsupersymmetric SO(10) models: An update," Phys. Rev. D **51** (1995) 229 [arXiv:hep-ph/9404238].

[23] H. Murayama and A. Pierce, "Not even decoupling can save minimal supersymmetric SU(5)," Phys. Rev. D **65** (2002) 055009 [arXiv:hep-ph/0108104].
B. Bajc, P. Fileviez Pérez and G. Senjanovic, "Proton decay in minimal supersymmetric SU(5)," Phys. Rev. D **66** (2002) 075005 [arXiv:hep-ph/0204311].
B. Bajc, P. Fileviez Pérez and G. Senjanovic, "Minimal supersymmetric SU(5) theory and proton decay: Where do we stand?," arXiv:hep-ph/0210374.
D. Emmanuel-Costa and S. Wiesenfeldt, "Proton decay in a consistent supersymmetric SU(5) GUT model," Nucl. Phys. B **661** (2003) 62 [arXiv:hep-ph/0302272].

[24] K. S. Babu and R. N. Mohapatra, "Predictive neutrino spectrum in minimal SO(10) grand unification," Phys. Rev. Lett. **70** (1993) 2845 [arXiv:hep-ph/9209215].
C. S. Aulakh, B. Bajc, A. Melfo, G. Senjanovic and F. Vissani, "The minimal supersymmetric grand unified theory," Phys. Lett. B **588** (2004) 196 [arXiv:hep-ph/0306242].
T. Fukuyama, A. Ilakovac, T. Kikuchi, S. Meljanac and N. Okada, "Detailed analysis of proton decay rate in the minimal supersymmetric SO(10) model," JHEP **0409** (2004) 052 [arXiv:hep-ph/0406068].
H. S. Goh, R. N. Mohapatra, S. Nasri and S. P. Ng, "Proton decay in a minimal SUSY SO(10) model for neutrino mixings," Phys. Lett. B **587** (2004) 105 [arXiv:hep-ph/0311330].

[25] T. Friedmann and E. Witten, "Unification scale, proton decay, and manifolds of G(2) holonomy," Adv. Theor. Math. Phys. **7** (2003) 577 [arXiv:hep-th/0211269].

[26] Agostinelli S et al. (Geant4 Collaboration) 2003 *Nucl. Instr. Meth.* A **506** 250

[27] Birks J M, *The theory and Practice of Scintillation Counting* (Pergamon Press, London, 1964)

[28] C. K. Jung, Feasibility a Next Generation Underground Water Cherenkov Detector: UNO, Preprint (arXiv:hep-ex/0005046) from the NNN99 Proceedings

[29] Hayaka T *Nucl. Phys.* B *(Proc. Suppl.)* **138** 376

[30] Kobayashi K et al. (Super-Kamiokande Collaboration) 2005 *(Preprint hep-ex/0502026)*

[31] A. S. Dighe and A. Y. Smirnov, Phys. Rev. D **62**, 033007 (2000).

[32] L. Cadonati et al., *Astropart. Phys.* 16 (2002) 361 and hep-ph/0012082 (2000)

[33] J. F. Beacom et al., *Phys. Rev.* D 66 (2002) 033001 and hep-ph/0205220 (2002)

[34] G. L. Fogli, E. Lisi, A. Mirizzi and D. Montanino, JCAP **0504**, 002 (2005).

[35] M. Kachelriess, R. Tomas, R. Buras, H. T. Janka, A. Marek and M. Rampp, Phys. Rev. D **71**, 063003 (2005).

[36] I. Gil-Botella and A. Rubbia, JCAP **0408**, 001 (2004) [arXiv:hep-ph/0404151].

[37] I. Gil-Botella and A. Rubbia, JCAP **0310**, 009 (2003)

[38] R. C. Schirato, G. M. Fuller, (. U. (. LANL), UCSD and LANL), astro-ph/0205390.

[39] G. L. Fogli, E. Lisi, D. Montanino and A. Mirizzi, Phys. Rev. D **68**, 033005 (2003).

[40] R. Tomas, M. Kachelriess, G. Raffelt, A. Dighe, H. T. Janka and L. Scheck, JCAP **0409**, 015 (2004).

[41] V. Barger, P. Huber and D. Marfatia, Phys. Lett. B **617**, 167 (2005).

[42] C. Lunardini and A. Yu. Smirnov, Nucl. Phys. B **616**, 307 (2001).

[43] A. S. Dighe, M. T. Keil and G. G. Raffelt, JCAP **0306**, 006 (2003).

[44] A. S. Dighe, M. T. Keil and G. G. Raffelt, JCAP **0306**, 005 (2003).

[45] C. Lunardini and A. Y. Smirnov, JCAP **0306**, 009 (2003).

[46] R. Tomas, D. Semikoz, G. G. Raffelt, M. Kachelriess and A. S. Dighe, Phys. Rev. D **68**, 093013 (2003).

[47] P. Antonioli *et al.*, New J. Phys. **6**, 114 (2004).

[48] A. Odrzywolek, M. Misiaszek and M. Kutschera, Astropart. Phys. **21**, 303 (2004).

[49] Ando, S. and Beacom, J. F. and Yuksel, H., *Phys. Rev. Lett.* 95 (2005) 171101, arXiv:astro-ph/0503321

[50] M. Fukugita and M. Kawasaki, Mon. Not. Roy. Astron. Soc. **340**, L7 (2003).

[51] S. Ando, Phys. Lett. B **570**, 11 (2003).

[52] G. L. Fogli, E. Lisi, A. Mirizzi and D. Montanino, Phys. Rev. D **70**, 013001 (2004).

[53] Malek, M. et al. [Super-Kamiokande Collaboration], *Phys. Rev. Lett.* 90 (2003) 061101, arXiv:hep-ex/0209028

[54] S. Ando, Astrophys. J. **607**, 20 (2004).

[55] Totani T, Sato K, Dalhed H E, Wilson J R*Astrophys. J.* **496** 216

[56] Thompson T A, Burrows A, Pinto P *Astrophys. J.* **592** 434

[57] Keil M, Raffelt G G, Janka H T *Astrophys. J.* **590** 971

[58] H. Yuksel, S. Ando and J. F. Beacom, arXiv:astro-ph/0509297.

[59] A. G. Cocco, A. Ereditato, G. Fiorillo, G. Mangano and V. Pettorino, JCAP **0412**, 002 (2004) [arXiv:hep-ph/0408031].

[60] Smy, M. B. [Super-Kamiokande Collaboration], Nucl. Phys. Proc. Suppl. 118 (2003) 25-32, arXiv:hep-ex/0208004

[61] G. Alimonti et al. [Borexino Collaboration], Astrop. Phys. 8, 141 (1998); ibid., *Nucl. Instrum. Methods* A406, 411 (1998)

[62] A. Ianni, D. Montanino, and F. L. Villante, *Phys. Lett.* B 627 (2005) 38

[63] A. Ianni, D. Montanino and F. L. Villante, *Phys. Lett.* B 627 (2005) 38, arXiv:physics/0506171

[64] P. Arneodo et al. [ICARUS], LNGS-P28/2001, LNGS-EXP 13/89 add. 1/01, ICARUS-TM/2001-03

[65] B. Aharmim *et al.* [SNO Collaboration], *Phys. Rev.* C 72 (2005) 055502, arXiv:nucl-ex/0502021

[66] M. C. Gonzalez-Garcia and Y. Nir, Rev. Mod. Phys. **75** (2003) 345 [arXiv:hep-ph/0202058].

[67] K. Daum *et al.* [Frejus Coll.], Z. Phys. C **66** (1995) 417.

[68] M. Aglietta *et al.* [NUSEX Coll.], Europhys. Lett. **8**, 611 (1989).

[69] R. Becker-Szendy *et al.* [IMB Coll.], Phys. Rev. D **46**, 3720 (1992).

[70] K. S. Hirata *et al.* [Kamiokande Coll.], Phys. Lett. B **280**, 146 (1992).

[71] Y. Fukuda *et al.* [Super-Kamiokande Coll.], Phys. Rev. Lett. **81**, 1562 (1998) [arXiv:hep-ex/9807003].

[72] W. W. M. Allison *et al.* [Soudan-2 Coll.], Phys. Lett. B **449**, 137 (1999) [arXiv:hep-ex/9901024].

[73] M. Ambrosio *et al.* [MACRO Coll.], Phys. Lett. B **517**, 59 (2001) [arXiv:hep-ex/0106049].

[74] Y. Ashie *et al.* [Super-Kamiokande Collaboration], Phys. Rev. D **71** (2005) 112005 [arXiv:hep-ex/0501064].

[75] M. H. Ahn *et al.* [K2K Coll.], arXiv:hep-ex/0606032.

[76] N. Tagg [MINOS Coll.], arXiv:hep-ex/0605058.

[77] Y. Itow *et al.* [T2K Coll.], arXiv:hep-ex/0106019.

[78] D. S. Ayres *et al.* [NOνA Coll.], arXiv:hep-ex/0503053.

[79] C. W. Kim and U. W. Lee, Phys. Lett. B **444** (1998) 204 [arXiv:hep-ph/9809491]; O. L. G. Peres and A. Y. Smirnov, Phys. Lett. B **456** (1999) 204 [arXiv:hep-ph/9902312].

[80] M. C. Gonzalez-Garcia and M. Maltoni, Phys. Rev. D **70**, 033010 (2004) [arXiv:hep-ph/0404085].

[81] T. Araki et al., "Experimental investigation of geologically produced antineutrinos with KamLAND," Nature **436** (2005) 499.

[82] S. Fukuda et al. [SuperKamiokande], *Nucl. Instrum. Methods* A501 (2003) 418-462

[83] A. Bueno, R. Cid, S. Navas-Concha, D. Hooper and T. J. Weiler, JCAP **0501**, 001 (2005) [arXiv:hep-ph/0410206].

[84] K. Eguchi et al. [KamLAND], *Phys. Rev. Lett.* 90 (2003) 021802; T. Araki et al. , arXiv:hep-ex/0406035

[85] S. Choubey and S.T. Petcov, *Phys. Lett.* B594 (2004) 333-346

[86] Autin, B. et al. , CERN-2000-012

[87] Gomez-Cadenas J. J. et al. , CERN working group on Super Beams (2001), arXiv:hep-ph/0105297

[88] Blondel A. et al. , *Nucl. Instrum. Methods* A503 (2001) 173-178

[89] Mezzetto M., J. Phys. G29 (2003)1781-1784, arXiv:hep-ex/0302005

[90] Apollonio M. et al. , arXiv:hep-ph/0210192

[91] Campagne J.-E. and Cazes A., Eur. Phys. J. C 45 (2006) 643, arXiv:hep-ex/0411062

[92] J. E. Campagne, M. Maltoni, M. Mezzetto and T. Schwetz, arXiv:hep-ph/0603172, submitted to *Phys. Rev.* D

[93] Campagne J.-E., arXiv:hep-ex/0510029

[94] Catanesi M.G. et al. [HARP Collaboration], CERN-SPSC/2001-017 SPSC/P322 May 2001

[95] M. Maltoni, T. Schwetz, M. A. Tortola and J. W. F. Valle, New J. Phys. **6**, 122 (2004) [hep-ph/0405172];

[96] Zucchelli P., Phys. Lett. B532 (2002) 166-172

[97] Mezzetto M., J. Phys. G29 (2003) 1771-1776, arXiv:hep-ex/0302007

[98] Bouchez J. and Lindroos M. and Mezzetto M., AIP Conf. Proc. 721 (2004) 37-47, arXiv:hep-ex/0310059

[99] Mezzetto M., Nucl. Phys. Proc. Suppl. 143 (2005) 309-316, arXiv:hep-ex/0410083

[100] Donini A. and Fernandez-Martinez E. and Migliozzi P. and Rigolin S. and Scotto Lavina L., Nucl. Phys. B710 (2005) 402-424, arXiv:hep-ph/0406132

[101] C. Rubbia, A. Ferrari, Y. Kadi and V. Vlachoudis, arXiv:hep-ph/0602032.

[102] Bernabeu J. and Burguet-Castell J. and Espinoza C. and Lindroos M., arXiv:hep-ph/0505054

[103] Sato J., Phys. Rev. Lett. 95 (2005) 131804, arXiv:hep-ph/0503144

[104] J. Burguet-Castell, M. B. Gavela, J. J. Gomez-Cadenas, P. Hernandez and O. Mena, Nucl. Phys. B **608** (2001) 301 [hep-ph/0103258]; H. Minakata and H. Nunokawa, JHEP **0110**, 001 (2001) [hep-ph/0108085]; G. L. Fogli and E. Lisi, Phys. Rev. D **54**, 3667 (1996) [hep-ph/9604415].

[105] Burguet-Castell J. and Casper D. and Couce E. and Gomez-Cadenas J. J. and Hernandez P., Nucl. Phys. B725 (2005) 306-326, arXiv:hep-ph/0503021

[106] Burguet-Castell J. and Casper D. and Gomez-Cadenas J. J. and Hernandez P. and Sanchez F., Nucl. Phys. B695 (2004) 217-240, arXiv:hep-ph/0312068

[107] Terranova F. and Marotta A. and Migliozzi P. and Spinetti M., Eur. Phys. J. C38 (2004) 69-77, arXiv:hep-ph/0405081

[108] Huber P. and Lindner M. and Rolinec M. and Winter W., arXiv:hep-ph/0506237

[109] Bruning O. et al. , CERN-LHC-PROJECT-REPORT-626

[110] Donini A. et al. , arXiv:hep-ph/0511134

[111] Lindroos M., EURISOL DS/TASK12/TN-05-02 to be published in Nucl. Phys. Proc. Suppl. (2006)

[112] A. Badertscher, M. Laffranchi, A. Meregaglia, A. Muller and A. Rubbia, Nucl. Instrum. Meth. A **555**, 294 (2005) [arXiv:physics/0505151].

[113] A. Bueno, M. Campanelli and A. Rubbia, Nucl. Phys. B **589**, 577 (2000) [arXiv:hep-ph/0005007].

[114] A. Bueno, M. Campanelli, S. Navas-Concha and A. Rubbia, Nucl. Phys. B **631**, 239 (2002) [arXiv:hep-ph/0112297].

[115] D. Mei and A. Hime, Phys. Rev. D **73** (2006) 053004 [arXiv:astro-ph/0512125].